Chapter 6

Regolith geochemistry

6.1. Introduction

Selective leaching or selective extraction analysis of soil samples is one of the more frequently applied geochemical methods in the identification of buried mineral deposits (Xueqiu, 1998;Gray et al., 1999; Cameron et al., 2004). This is a partial extraction method, which only dissolves part of the weakly absorbed and, or adsorbed elements of interest in a particular solution. This method is also effective in identifying highly soluble new mineral phases that may form in the secondary environment including phosphates, chlorides and carbonates. The soluble part of the sample represents the "mobile" phases, referred to as mobile metal ions (MMI) (Mann et al., 1998; Cameron et al., 2004; Mann et al., 2005), which could have been derived from a weathering ore deposit. In nature, the water cycle and secondary processes cause the metal ions to be leached from the rock and ore deposit and to become precipitated in the soil.

The secondary soil forming processes may form a gossan at the top of massive sulphide deposits by reduction and oxidation weathering processes and a calcrete layer near the surface by evaporation of soil moisture during the diurnal cycle (under arid to semi-arid conditions). In the study area, a layer (of variable thickness ranging from zero to several meters) of wind blown sand covers this calcrete layer that in itself varies from zero to 6 m or more.

The main objective of this chapter is to investigate nature's ability to impart a secondary geochemical dispersion halo to a non-residual wind blown sand cover above a massive sulphide ore body and to determine to what extent the intermediate calcrete layer acted as

a geochemical barrier to this process. For this, wind blown sand (Kalahari sand) samples were collected along regolith sampling traverses in the research areas. Different types of selective leach methods and total analyses are used to determine if an anomaly related to the mineralization may be detected, and which method is the most appropriate for this. The results of selective extraction methods are also compared to total analysis by x-ray fluorescence (XRF) results to identify the method which gives the highest anomaly to background ratio and widest dispersion.

The calcrete layer, as part of the secondary environment, is investigated by samples collected from surface and at different depths in the calcrete layer to investigate the variation in the concentration of some trace elements in this potential barrier to geochemical dispersion. The objective with this is to determine whether a lithogeochemical survey of calcrete samples would be successful in detecting underlying massive sulphide mineralization.

The principal aspects that would be addressed in this chapter are:

a) An experiment to determine the most appropriate reagents to use for detecting the concealed ore bodies in the sand cover at surface.

b) A comparison of the best reagent partial extraction method with a total analysis method (XRF).

c) The distribution of the elements of interest in the calcrete layer.

6.2. The concept of mobile metal ions and selective extraction techniques

In theory, it could be argued that partial extraction or selective extraction methods, when applied to soil geochemistry in exploration programmes, may provide a better selection of "true" anomalies and also result in a better definition of the secondary dispersion haloes related to concealed massive sulphide ore bodies (Levinson, 1974). Such definition may be defined by larger peak to background ratios and, or a larger anomalous area (dispersion area) that could be detected. Initially these methods were hampered by the relatively high (ppm) lower limits of detection of the standard analytical methods

commonly used (mostly atomic absorption techniques). But since the advent of inductively coupled plasma, optical emission spectrometry (ICP-OES) and especially with the introduction of inductively coupled plasma mass spectrometry (ICP-MS) the detection of very low concentrations of various elements in solution (ppb range) has become a viable method for exploration geochemical application. Simultaneous advances in total analytical techniques such as XRF has also lowered the detection limit of this technique although still much less sensitive than the ICP techniques. These two methods would be compared in the following sections.

6.2.1. Mobile Metal Ions (MMI) concept

"Mobile Metal Ions" is a term that describes ions that have migrated into the weathering zone, and are only weakly or loosely attached to the surfaces of the soil particles (Mann et al., 1998; Cameron, et al., 2004; Mann et al., 2005). These ions have the ability to disperse through un-mineralized rock e.g. hundreds of meter vertically upwards (Genalysis Laboratory Services Pty Ltd, 20th January, 2005) possibly by poorly understood micro-bubbles, vapor, ground-water flow, capillary rise or electrochemical processes (Cameron et al., 2004; Mann et al., 2005). The convection cells set up by rainfall and evaporation during the rainfall and dry periods, respectively, are also contributing to the movement of mobile ions into the soil traverses (Figure 6.1).

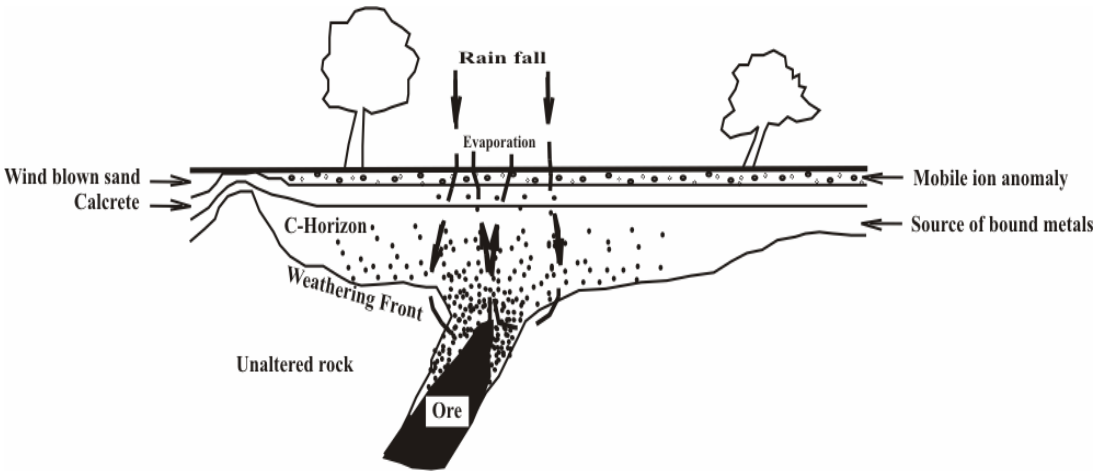

Figure 6.1: Schematic model of convection cell in connection with mobile metal ions in the secondary environment (after Mann et al., 1997)

Mann et al. (1995) and Mann et al. (1997) carried out experimental work to determine the vertical movement of mobile elements and the effect a calcium carbonate layer would have on the movement of these mobile ions. In the first experiment (without

addition of calcium carbonate), coarse silica sand was added to a flower pot partially filled with a solution containing base metals. The metals in the solution were shown to move vertically upwards through the silica sand in a very short peroide (Mann et al., 1995; Mann et al., 1997). In the second experiment, varying quantities of calcium carbonate were added as a single layer to a pot with a solution and coarse silica sand as in the first experiment. In both experiments i.e. with or without carbonate added, a surface accumulation of mobile metals was observed. Thus it suggests that carbonate, a known precipitant of base metals, has not inhibited the surface response or the movement of the base metals (Mann et al., 1995; Mann et al., 1997).

The elements that have migrated due to soil forming processes may be derived from two sources, i.e., from an endogenic or exogenic source. Elements from an endogenic source are derived from primary minerals, which are not directly related to the mineralization. These elements are referred to as bound elements as they are not dissolved by digestant or selective extractants (Bardshaw et al., 1974; Leinz et al., 1993). Elements from an exogenic source are derived from the disintegration of the ore minerals (sulphides) related to the mineral deposits, due to natural oxidation processes (Cameron et al., 2004). The term unbound elements are used for these metals as they can be extracted by a digestant or detached from soil. Mobile ions are therefore unbound elements, which are concentrated in the A horizon of a soil profile. Bound elements originate from the C-horizon and get concentrated in the B-horizon in the event of low rainfall and infiltration (Mann et al., 1995; Mann et al., 1997). In this investigation, Cu, Zn, Pb, Fe, Mn, Ba and S are considered elements of interest, as they are directly related to the ore and it will be attempted to determine if they behave mobile and are detectable in the Kalahari sand overlying the deposit.

According to Goldberg (1998), mobile metal ions may occur in surface environments in one of the following forms:

-aqueous forms e.g. ionic, colloidal, etc;
-adsorbed onto the mineral surfaces or soil colloids;
-adsorbed onto organic matter, certain metal-organic complexes;
-as soluble sulphates, carbonates, phosphates, etc; or
-adsorbed onto oxides and hydroxides of Fe and Mn.

Unfortunately major rainfall events or periodic flooding in soils are accompanied by loss of such mobile metal ions, because these events have the capacity to remove weakly bound metals from soils (Genalysis Laboratory Services Pty Ltd, 20th January, 2005). This is the reason for not sampling soon after major rainfall events unless data to the contrary exists. The samples for this study were collected during the dry season (winter) of 2003.

6.2.2. Selective extraction techniques

The purpose of selective extraction is to leach only the mobile metal ions of the sample matrix. These methods are designed to attack specific components within a sample. Some methods dissolve precipitated carbonates or other salts, while others attack Mn-oxides, amorphous Fe-oxides, or extract metal ions held in organic complexes. The base of these extractants is an acidic solution, but the intensity of pH determines which elements will be leached from the sample. Weaker acid affects the exogenic phase and in order to dissolve the endogenic phase, a stronger acid has to be used. In general, most metals become more soluble at low pH values (Maes, 2003).

In Table 6.1, different extractants are classified based on their chemical power or acidity. These extractants may be used in a sequential leaching process from the top to the bottom of this table i.e. starting with the weakest solutions. Other extractants are given in Table 6.2, which may be used for selective leaches. Some of the selective extraction methods for Cu, Zn, Pb, Cd and S in soil samples are listed in Table 6.3.

The ions in the extraction solution generally occur in very low, typically parts per billion (ppb) concentrations and this require a low detection technique such as ICP-MS to determine the mobile metal content (Wang, 1997). The ICP-MS technique is also used here to determine the concentration of the elements of interest in the various solutions prepared.

Table 6.1: Different extractants classified be acidity (sequential leaching process and/or selective leaches)

Extractant	Effects	Classification	Examples	References
Deionized water	does not attack any minerals, but removes elements loosely adsorbed on mineral surfaces	This solution dissolves water-soluble salts and elements loosely adsorbed on mineral surfaces.		Cameron et al., 2004
Enzyme leach (dilute glucose solution)	Removes the MnO coating found on all clay crystals. It forms oxidation halo anomalies.	This leach dissolves little more than deionized water, but gives better analytical reproducibility (Electrically migratable atoms)	To detect reduced mineral deposits such as porphyry Cu, Oil and gas reservoirs	Clark and Russ, 1992; Clark, 1997; Cameron et al., 2004
Mobile Metal Ions (MMI)	Dissolves secondary minerals	1. MMI-A (acidic) 2. MMI-B (Basic) 3. MMI-C (Carbonate) 4. MMI-D (diamonds) 5. MMI-E 6. MMI-F 7. MMI-G (granophiles)	1.Base metals (Cu, Pb, Zn, Cd) 2.Precious metals (Au, Ag, Ni, Co, Pd [Pt]) 3.Base metals (Cu, Pd, Zn, Cd) 4.Kimberlites (Ni, Nb, Cr, Mg, Fe, Mn) 5.Majors mineral sands (Ti, Fe, Si, Mg, Ca, Th, Zr, Sc) 6.Path finders (As, Sb, Mo, W) 7.Pegmatophiles (U, Pb, Th, Sn, Li, Ta)	Cameron et al., 2004
Ammonium acetate	Dissolves carbonate minerals (pH= 5)	Use a leach that dissolves one or more secondary minerals that contain a favourable ratio of exogenic/endogenic material		Cameron et al., 2004
Hydroxylamine hydrochloride (HX)	For oxide minerals (It affects two phases: Carbonate and water-soluble minerals)	1. Cold Hydroxylamine 2. Hot Hydroxylamine	1. {pH=1.5, room temperature}(HX Mn) : carbonate and water-soluble minerals 2. {pH= more strongly acidic, T=60^{0}C}(HX Fe) : carbonate and water-soluble	Cameron et al., 2004
Aqua-regia ($HCl + HNO_3$)	Most of the secondary minerals and some of the silicates	It is not a selective leaching analysis.	Gold reacts only with the concentrated acid mixture which is referred to as aqua regia (royal water)	Cameron et al., 2004
$HF+HClO_4+HNO_3+HCl$	Silicates, residual crystalline fraction	It is not a selective leaching analysis.	Refractory minerals could remain in the final residual	Cameron et al., 2004

Table 6.2: Some other extractants for selective leaching

Extractants	Effects	Classification	Examples/ (References)
Sodium pyrophosphate	Dissolves large amounts of endogenic metals or those unrelated to the mineralization	Organic material, humus	
Regoleach	Dissolves metal ions adsorbed on clay surfaces, those attached to organic material, and those combined with amorphous Fe and Mn oxides	Strongly attack most metals	Moderate-strength leach Au, pathfinder and indicator (W, U, REE, et.) in a wide range of sample materials and base metal
Ethylene Diamine tetraacetic acid (EDTA)	To extract metals freshly adsorbed onto organic matter, metals from Fe-oxide or Fe-hydroxide species and to release metals by dissolution of carbonates		(Luoma and Jenne, 1976; Miller et al., 1986; Miller and McFee, 1983; Stover et al., 1976)
Ammonium citrate	To attack metals adsorbed on organic and clay particles		
Ammonium citrate and dilute hydrochloric acid	To attack some of the metals bound on Mn oxide		

Table 6.3: Selective extraction methods for Cu, Zn, Pb, Cd and S in the soil

Element	Form	Method of extraction
Cu and Zn in soil [1]	-As free and complexed ions, adsorbed cations (exchangeable cations), ions occluded mainly in soil carbonates and hydrous oxides; in biological residues and living organisms and in the lattic structure of primary and secondary minerals. -These elements are absorbed by carbonates, soil organic matter, phyllosilicates, and hydrous oxides of Al, Fe, and Mn. Cu and Zn are more concentrated in silty or clayey soils than in sandy soils	-Diethylenetriaminepentaacetic acid-Trithanolamine (DTPA-TEA) and Diethylenetriaminepentaacetic acid-NH_4HCO_3 (DTPA-AB) Method: To identify near-neutral and calcareous soils with insufficient levels of available Cu, Fe, Mn and Zn; -Mehlich-I (double acid) Method: The EDTA result for Zn has a high correlation with the result of this method; and - Mehlich-I Method: Solution includes EDTA to extract the available Cu, Mn, and Zn.
Pb and Cd in soil[2]	The content is quite low except in areas where the parent material has high levels of these elements or air pollution and land disposal of industrial and municipal wastes occur.	-Exchangeable phase: NH_4OAc (pH=7, buffered salts) -Carbonate-bound metals: NaOAc (pH=5, 1M) NH_4OAc (pH=4.5,1M) -Organic matter and metal oxides: NaOCl; $Na_4P_2O_7$
Cu, Zn and Pb in soil[3]	-As adsorbed, exchangeable metals and dissolution of phases.	-20 g of soil sample + 50 ml of 1 M NH_4NO_3[3] (to determine concentrations of Ag, As, Bi, Co, Cr, Cu, Hg, Mn, Mo, Ni, Pb, Sb, Tl, U, V and Zn in soil).
S (sulfur) in soil[4] (Most soils contain 100 -500 mg kg^{-1})	1) Inorganic S ($SO4^{2-}$, S^{2-}, Sn^{2-}, $SO3^{2-}$, $S_2O_3^{2-}$): They may occur as water-soluble salts (in arid regions), adsorbed by soil colloids (on kaolinite clay, Fe and Al oxides), or insoluble form (include Ba and Sr sulfates, sulfate coprecipitate with $CaCO_3$, and basic Fe and Al sulfates) in soils 2) Organic S: >.95 % of the total S in humid and semi humid regions is organic sulfur.	1-a) Soluble sulfate: extractable with H_2O and salt solutions containing NaCl, LiCl, or $CaCl_2$ 1-b) Adsorbed sulfate shaking with $NaHCO_3$, $CaCO_3$ suspensions, NH_4OAc (1M, pH=7), acidic NH_4OAc, Morgan's solution and $Ca(H_2PO_4)_2$ (0.01 M). 2) In this investigation is not important.

1-Liang et al., 1991; Soltanpour, 1991; Kabata-Pendia and Pendias, 1991;Neilsen et al., 1986; Mehlich, 1984; Soltanpur et al., 1982; Iyengar et al., 1981; Schnitzer, 1978; Lindsay and Norvell, 1978; Wear and Evans, 1968.

2-Adriano, 1986; Miller et al., 1986; Salomons and Forstner, 1984; Chao, 1984; Shuman, 1983; Tessier et al., 1979.

3-Hall, et al., 1998 4-Tabatabai and Laflen, 1976a, b;Alymore et al., 1967; Fox et al., 1964; Stanford and Lancaster, 1962; Williams and Steinbergs, 1962; Chao et al., 1962a, Kilmer and Nerrpass, 1960; McClung et al., 1959.

6.3. Sampling programme

To investigate the secondary geochemical dispersion haloes in non-residual sand, a total of 102 samples were taken from the surface at the Kantienpan and Areachap deposits. The sampling programme involved three regolith traverses from Kantienpan (18 samples from KP5, 16 samples from KP8 and 19 samples from KP12) and three regolith traverses from Areachap (20 samples from T1, 21 samples from T2 and 8 samples from T3). The location of the regolith traverses from Kantienpan and Areachap are shown in Figures 6.2 and 6.3. Sample intervals are 10 m near the projected position of the mineralized zone and increase to 20, 50 and 100 m further away from this zone.

The calcrete layer that may act as a potential geochemical barrier to the dispersion of the elements of interest and which also forms part of secondary environment was also

investigated. For this, a total of 14 samples of approximately 3 kg each were collected from the calcrete layer in the two areas under investigation. Six calcrete samples were collected from the surface near the gossan zone at Kantienpan (Fig. 6.2), together with two calcrete samples (outside the Kantienpan geology map) further away from the ore zone. All of the samples collected from directly above the ore zones contained inclusions of gossan materials. The latter are used for comparisons. Six calcrete samples were collected in two depth profiles from an old excavation at Areachap (Fig. 6.3), each profile includes three samples. A Frantz isodynamic magnetic separator was used to separate the magnetic part of calcrete samples by varying the electric current flowing through the electromagnet (Appendix D). Mineralogical phases in the magnetic and non-magnetic parts of one sample (KP12/4) were determined by x-ray diffractometry (XRD) and element concentrations in the magnetic, non-magnetic and original sample were analyzed by XRF.

6.4. Selection of the most appropriate extraction reagent

To generate results and identify a method that would be commercially viable in a general exploration application, it was decided to use the standard reagents freely available and not to use expensive spectroscopically pure reagents, nor to engage in stringent cleaning procedures for the reagents. In the current research, the extractants selected from the tables (Tables 6.2 and 6.3) included ammonium nitrate (NH_4NO_3) (Table 6.3), ammonium acetate (NH_4OAC) (Table 6.3), ethylene diamine tetraacetic acid (NH_4EDTA) (Tables 6.2 and 6.3) and calcium hydro-phosphate ($Ca(H_2PO_4)_2$) (Table 6.3) were all tested to find the best extracting solution for the mobile metal ions from the sand samples. The results obtained (see Appendix D) show that the NH_4EDTA solution provide the most reliable results and that this reagent could be used to extract the mobile metal ions such as Cu, Zn, Pb, Mn and Fe with an optimum shaking time of 180-minutes. $Ca(H_2PO_4)_2$ solution represent a successful reagent that may be used to extract the S in the samples with an optimum shaking time of 120-minutes.

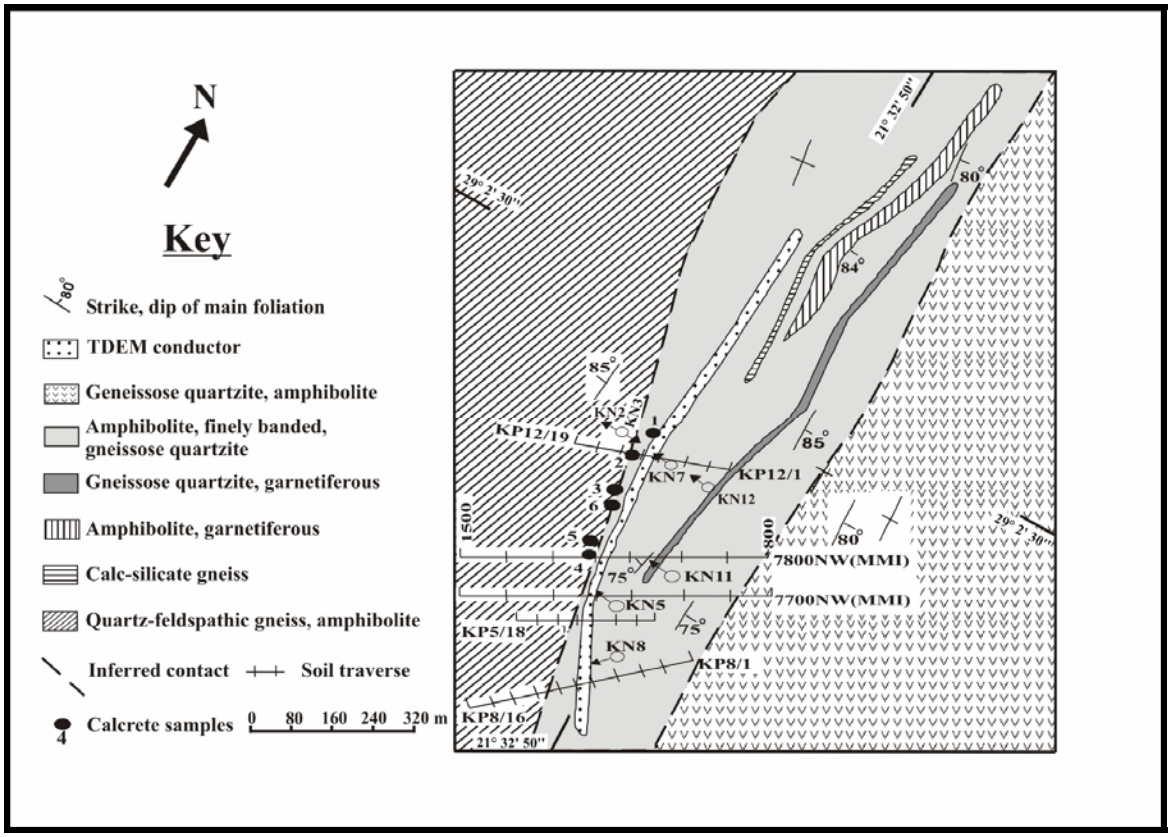

Figure 6.2: Regolith traverses and geology map of the Kantienpan area (after Rossouw, 2003)

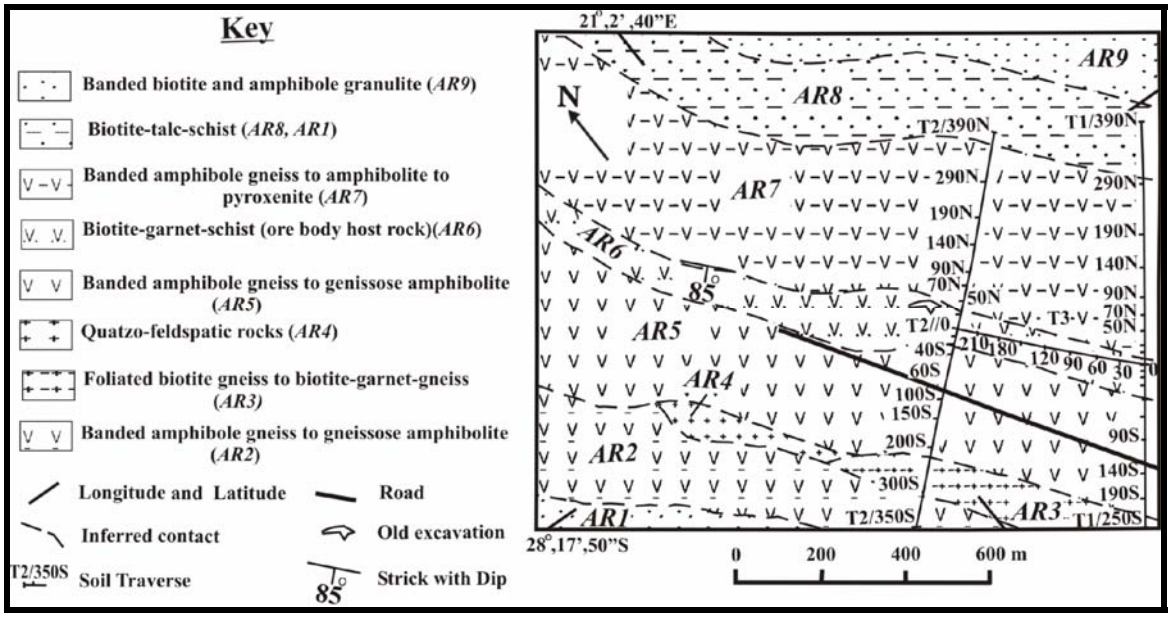

Figure 6.3: Regolith traverses and geology map of the Areachap area (after Voet and King, 1986)

6.5. Calculation of the threshold value for the anomalous population

To discriminate and define the dispersion zone related to a concealed ore deposit, the threshold value for the anomalous samples has to be determined. For this purpose, the type of statistical distribution and the number of populations (polimodality) has to be investigated before the calculation of the threshold values could be attempted.
SAS software (SAS® version 8.2) was used to test the normality of the population. The null hypothesis for this test is that the input data values are a random sample from a normal distribution (SAS® version 8.2). For sample sizes greater than six, the Shapiro and Wilk (1965) value (W) is computed. If the W statistic is very small, then the normality hypothesis is rejected (Shapiro and Wilk, 1965). By definition, a normal distribution should have the same mean, median and mode, and both the skewness and kurtosis should be equal to zero (SAS® version 8.2).

If the results of the test and probability plot of the data shows a single normal or lognormal population, then the mean plus one and/or two standard deviations may be used as the threshold value. Where the results show more than one population, the Probplot software application of Sinclair (1976) is used to separate the anomalous sub-population and to calculate the lower threshold value for this sub-population.

In the following sections, the threshold value calculation is explained for different partial extractions and total analyses results.

6.5.1. The threshold value for NH_4EDTA extraction

The NH_4EDTA solution was used to extract the mobile metal ions in 52 sand samples from Kantienpan. The extracts were analyzed by ICP-MS and the results are listed in Appendix D, Tables D.12-D.14. To arrive at a statistically valid interpretation, a data set that includes all the analytical results is used to perform the test for normality. Based on Table 6.4, all the elements have a lognormal population (the log values have the highest W value). The mean, median and mode of the log values are nearly the same, and their skewness and kurtosis in most of elements are very close to zero, confirming that the samples display a lognormal distribution.

Table 6.4: Results of the normality test for the data from Kantienpan (ICP-MS method, n = 52)

Element	Shapiro-Wilk		Mean	Median	Mode	Skewness	Kurtosis
	W	Pr<W					
Pb	0.2918	<0.0001	7.5	3.5	3	6	39
Log Pb	0.7359	<0.0001	1.4	1.2	1.1	2.4	69
Zn	0.9113	0.0009	5144.5	4925.5	5654	1.19	2.31
Log Zn	0.9655	0.1350	5.3	5.4	4.4	-0.27	-0.77
Cu	0.8625	<0.0001	4297.4	3914	0	1.65	3.57
Log Cu	0.9663	0.1469	8.3	8.3	0	0.55	0.77
Mn	0.9427	0.0144	217.7	211.5	80	0.63	-0.27
Log Mn	0.9655	0.1350	5.3	5.4	4.4	-0.27	-0.77
Ba	0.8866	0.0001	23.9	22	22	1.48	2.98
Log Ba	0.9608	0.0850	3.1	3.1	3.1	0.71	0.72

The probability plots of the log values for each element are shown in Figure 6.4. A linear trend in the plots for each element may be used as proof for a single lognormal distribution.

Results indicate an effective detection limit of 2 ppm Pb, probably reflecting the background concentration in the reagents used. To obtain a more amicable distribution of the population, it was decided to substitute the value, for samples returning concentrations equal to the effective detection limit, with zero.

The single lognormal distribution of elements may be related to the ore forming process and indicate that the elements investigated may be regarded as derived from an exogenic source. All samples returning concentrations higher than the threshold value (Mean ± standard deviation or Mean ± two times the standard deviation) is regarded as anomalous. The statistical calculations for the mean, standard deviation, and threshold values for each element are summarized in Table 6.5. The mean and standard deviation of untransformed data is used. Blank values reported reflect the concentration of the elements in the NH_4EDTA reagent solution.

Table 6.5: The threshold values of elements in the Kantienpan data set (ICP-MS method, n=52 samples).

Element	Mean (M)	Standard deviation (SD)	Blank value	Threshold values	
				M + SD	M + 2*SD
Cu (ppb)	4297	1470	400	5768	7238
Zn (ppb)	5145	2044	1742	7189	9233
Pb (ppm)	7	17	163 (ppb)	24	41
Mn (ppm)	218	109	2	327	436
Ba (ppm)	24	6	410 (ppb)	30	36

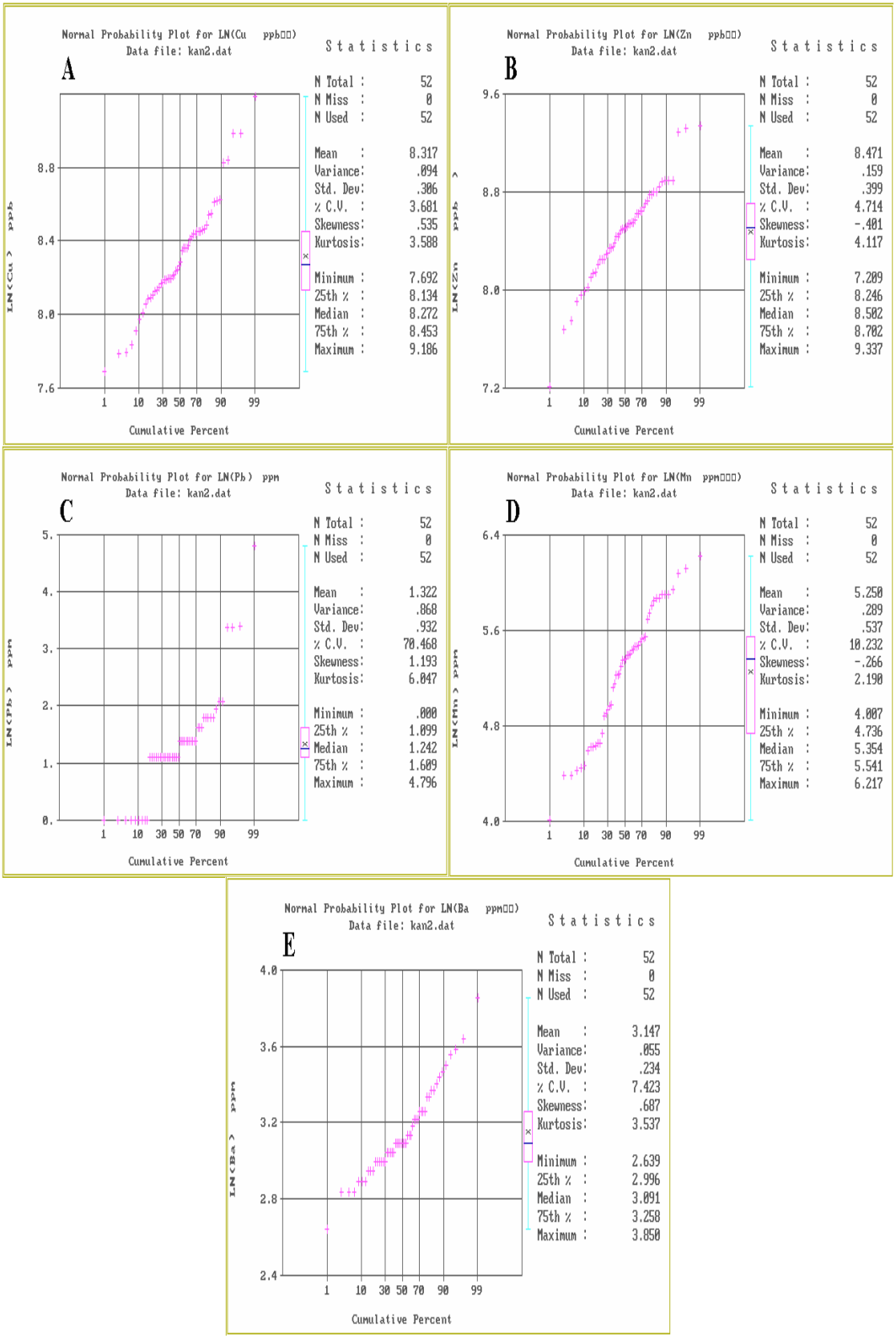

Figure 6.4: Probability plot of the log values for Cu (A), Zn (B), Pb (C), Mn (D) and Ba (E), whole Kantienpan regolith data set (ICP-MS method, n=52 samples).

The NH_4EDTA solution was also used to extract the mobile metal ions in 61 sand samples from Areachap. The extracts were analyzed by ICP-MS (Appendix D, Tables D.16 to D.18), and a regolith data set including these analytical results was used for the normality test, by using the univariate procedure (Table 6.6). Based on the normality test, all elements have lognormal distribution, as the log values have the highest W value. This is also supported by the mean, median and mode of the log vales which are nearly the same, and the skewness and kurtosis for most elements that are very close to zero.

Table 6.6: The results of the normality test for the data set from Kantienpan (ICP-MS method, n = 52)

Element	Shapiro-Wilk		Mean	Median	Mode	Skewness	Kurtosis
	W	Pr<W					
Cu (ppb)	0.5869	<0.0001	4928	2420	0	3.2	11.1
Log Cu	0.9128	0.0004	8	7.8	0	0.9	0.5
Zn (ppb)	0.7390	<0.0001	7577	5180	0	2.4	6.5
Log Zn	0.9527	0.0194	8.7	8.6	0	0.5	-0.3
Pb (ppb)	0.8083	<0.0001	2572	2119	0	1.9	3.9
Log Pb	0.9435	0.0072	7.8	7.7	0	0.8	0.2
Mn (ppm)	0.8848	<0.0001	112	106	44	1.5	3.8
Log Mn	0.9719	0.1737	4.6	4.7	3.8	-0.02	-0.4
Fe (ppm)	0.8457	<0.0001	79	74	64	1.8	3.7
Log Fe	0.9401	0.0050	4.3	4.3	4.2	1	1

The probability plots of the log values for each element are shown in Figure 6.5. The linear trend of the data for each element may be interpreted as proof of a single lognormal distribution. The low values in the Cu probability plot may be due to the background effect i.e., the concentration in the reagent solution.

The single lognormal distribution of elements may be related to the ore forming process and indicate that the element investigated may be regarded as derived from an exogenic source. Statistical calculations for the mean, standard deviation, and threshold values are summarized in Table 6.7.

Table 6.7: The threshold values for whole Areachap data set (NH_4EDTA method, n=61).

Element	Mean (M)	Standard deviation (SD)	Blank values	Threshold values	
				M + SD	M + 2*SD
Cu (ppb)	4928	3411	47-74	8339	11750
Zn (ppb)	7577	6314	670-819	13891	20205
Pb (ppb)	2572	1290	<1-17	3862	5152
Mn (ppm)	112	59	≈1	171	230
Fe (ppm)	79	22	2-61	101	123

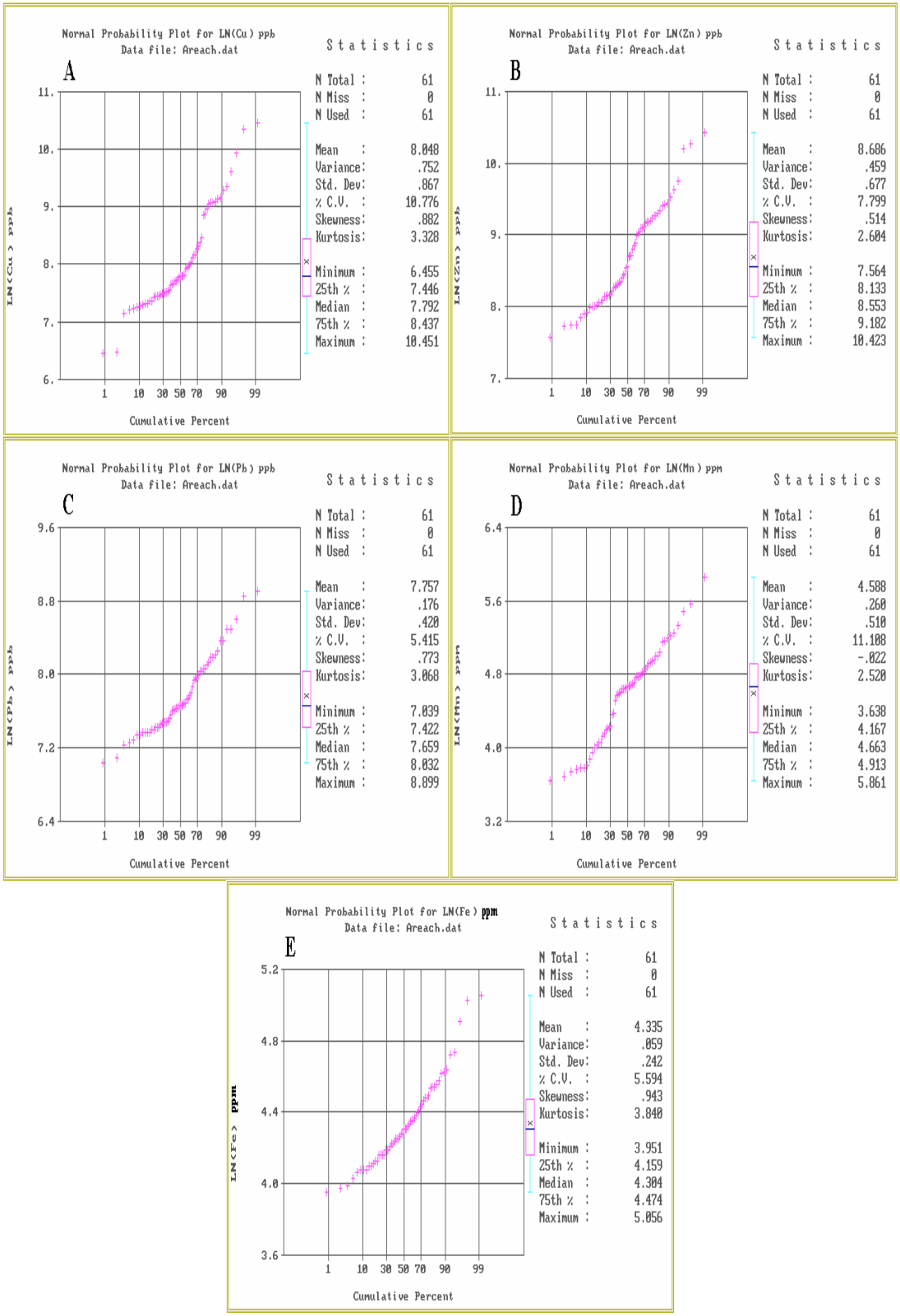

Figure 6.5: Probability plot of the log values for Cu (A), Zn(B), Pb(C), Mn (D) and Fe (E), whole Areachap regolith data set (ICP-MS method, n=61 samples).

6.5.2. The threshold value for $Ca(H_2PO_4)_2$ extraction

$Ca(H_2PO_4)_2$ solution was used to extract S from 33 sand samples from Kantienpan. The extracts were analyzed by ICP-MS and the results are given in Appendix D,

Tables D.7, D.9 and D.12. A regolith data set of these analyses is used for the normality test. The results of the statistical test for normality are given in Table 6.8. S has lognormal distribution, as the log values have high W value, and the mean, median and mode of the log vales are nearly the same.

Table 6.8: The normality test of distribution of S in Kantienpan data set (ICP-MS method, n = 33 samples)

Element	Shapiro-Wilk		Mean	Median	Mode	Skewness	Kurtosis
	W	Pr<W					
S (ppm)	0.4387	<0.0001	21	10	8	3.8	16.1
Log S	0.7033	<0.0001	2.6	2.3	2.1	2.1	3.9

The probability plot of the log values for S is shown in Figure 6.6. Two linear trends are present, one for low and the other for high values of S. This indicates an effective detection limit of 7-8 ppm S, probably reflecting the background concentration in the reagents used (Table 6.9). To obtain a more amicable distribution of the population, it was decided to substitute the value, for samples returning concentrations equal to the effective detection limit, with zero. The distribution of the rest of the samples approach a single lognormal distribution.

Table 6.9: S values for samples within and outside the halo and blank sample, Kantienpan and Areachap.

S (ICP-MS results, ppm)				
Blank sample	Outside the halo		Within the halo	
	Kantienpan	Areachap	Kantienpan	Areachap
5-6	9-10	7-10	90-180	12-20

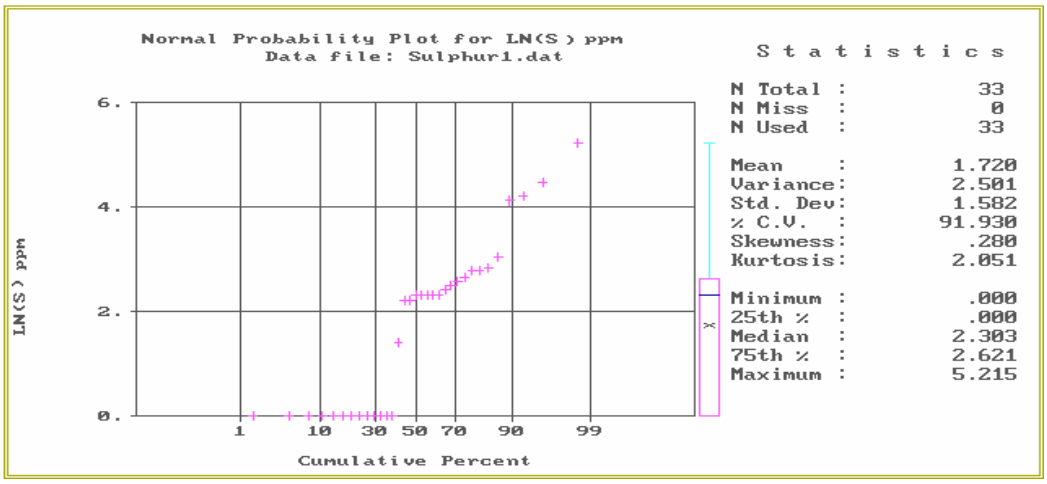

Figure 6.6: Probability plot of S, Kantienpan ($Ca(H_2PO_4)_2$, shaking time of 120-minutes, ICP-MS method)

The statistical calculations of the mean, standard deviation, and threshold values for S are summarized in Table 6.10.

Table 6.10: The threshold values of S for the Kantienpan data set (ICP-MS method, n=33 samples).

Element	Mean (M)	Standard deviation (SD)	Blank value	Threshold values	
				M + SD	M + 2*SD
S (ppm)	18	36	5-6	54	90

$Ca(H_2PO_4)_2$ solution was also used to extract S from 21 sand samples from Areachap. The extracts were analyzed by ICP-MS and the results are listed in Appendix D, Table D.18. Descriptive statistics of the data set and the results of the normality test are given in Table 6.11. The log values for S have a high W value suggesting that it has a lognormal population. This is confirmed by the similar values for the mean, median and mode of the log vales. The straight line distribution on the probability plot (Fig. 6.7) confirms this interpretation.

Table 6.11: The normality test for the distribution of S in the Areachap data set (ICP-MS method, n = 21 samples)

Element	Shapiro-Wilk		Mean	Median	Mode	Skewness	Kurtosis
	W	Pr<W					
S (ppm)	0.9448	0.2703	12	11	14	0.7	0.2
Log S	0.9708	0.7504	2.4	2.4	2.6	0	-0.4

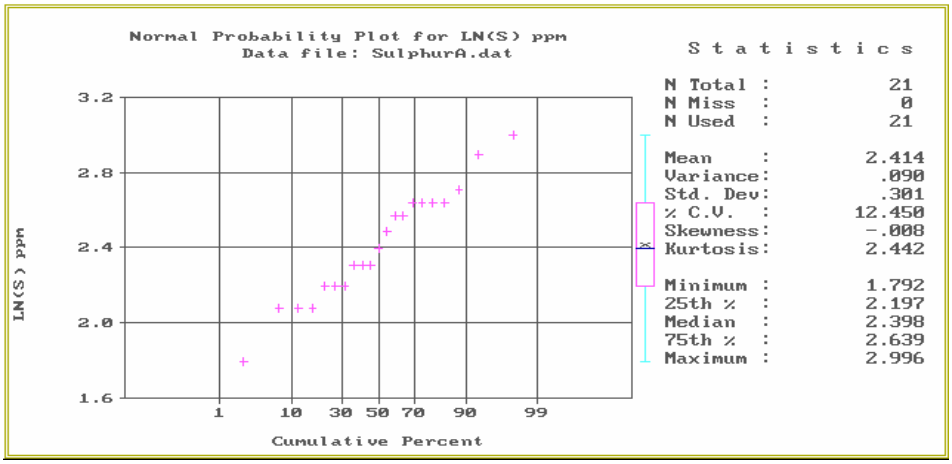

Figure 6.7: Probability plot of S, Areachap ($Ca(H_2PO_4)_2$, shaking time 120-minutes, ICP-MS method).

Table 6.12 summarizes the statistical parameters and threshold values for S at Areachap.

Table 6.12: The threshold values of S for the Areachap data set (ICP-MS method, n=21 samples).

Element	Mean (M)	Standard deviation (SD)	Threshold values	
			M + SD	M + 2*SD
S (ppm)	12	4	16	20

6.5.3. The threshold value for MMI-A analyses results

Rossouw (2003) sampled two traverses in the Kantienpan area, and submitted them for Cu and Zn analyses using the patented MMI-A method (Appendix D, Table D.15, and Table 6.1). The data is considered here in order to compare the results of the MMI-A results with the other methods, which were applied in the current research.

Table 6.13 summarizes the results of statistical tests for normality on the normal and log values of Cu and Zn. Cu has a normal and Zn has a lognormal distribution, which is confirmed by the calculated statistical parameters listed in this table.

Table 6.13: Results of the normality test (MMI method, n = 58 samples).

Element	Shapiro-Wilk		Mean	Median	Mode	Skewness	Kurtosis
	W	Pr<W					
Cu (ppb)	0.8740	<0.0001	61.5	65.1	1.9	1.3	4.9
Log Cu	0.7483	<0.0001	3.5	4.2	0.6	-1.1	-0.3
Zn (ppb)	0.4192	<0.0001	435	270	270	5.4	34.1
Log Zn	0.9590	0.0480	5.6	5.6	5.6	0.6	1.5

The probability plot of the normal (Cu) and log values (Zn) of the elements are plotted in Figure 6.8 A and B. The lowest values in the Cu probability plot (Fig. 6.8 A), may be due to the detection limit of the method. This may also explain the high kurtosis of Cu in Table 6.13. Based on these results, Cu has a single normal distribution and Zn has a single lognormal distribution.

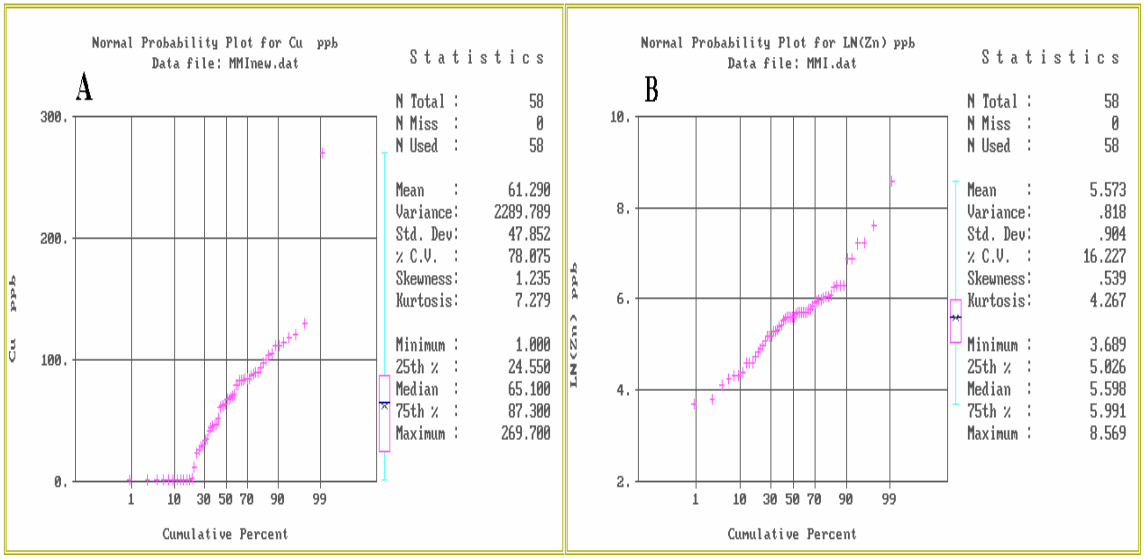

Figure 6.8: Probability plot of the normal and log values for Cu (A) and Zn (B) (MMI method, n=58 samples).

The statistical calculations of the mean, standard deviation, and threshold values for Cu and Zn determined with the MMI-A method are summarized in Table 6.14.

Table 6.14: The threshold values of Cu and Zn (MMI method, n=58 samples).

Element	Mean (M)	Standard deviation (SD)	Threshold values	
			M + SD	M + 2*SD
Cu (ppb)	61	48	109	157
Zn (ppb)	435	733	1168	1901

6.5.4. The threshold value for total analyses (XRF method)

To compare the results of the partial extraction analyses (NH_4EDTA and Ca $(H_2PO_4)_2$ solutions) with the total (XRF) analyses, samples of one regolith traverse from Kantienpan (KP12) and one from Areachap (T2) were also analyzed by XRF. (Appendix D, Table D.10 and D.11). The outcome of the normality test and other statistics for Cu, Zn, Pb, MnO and S obtained from XRF analyses of the Kantienpan samples are summarized in Table 6.15. Based on these results, Cu, Pb and MnO show normal distributions, whereas Zn and S display lognormal distributions.

The probability graphs of the normal and log values of the elements are given in Figure 6.9. Based on these it may be concluded that, Cu, Pb and MnO have single normal distributions and S has a single lognormal distribution. The results indicate an effective lower detection limit of 16 ppm S, probably reflecting the detection limit of the XRF method. To obtain a more amicable distribution of the population, it was

Table 6.15: Results of the normality test for regolith traverse of KP12 (XRF method, n = 19).

Element	Shapiro-Wilk		Mean	Median	Mode	Skewness	Kurtosis
	W	Pr<W					
Cu	0.9623	<0.6175	25	25	22	-0.64	1.1
Log Cu	0.8912	<0.0338	3.2	3.2	3.1	-1.46	3.77
Zn	0.8827	0.0239	108	102	94	0.62	-1.2
Log Zn	0.9016	0.0520	4.7	4.6	4.5	0.49	-1.25
Pb	0.9338	<0.2037	16	15	15	0.30	0.08
Log Pb	0.9322	0.1899	2.8	2.71	2.71	-0.43	1.19
MnO	0.892	0.0356	0.1	0.09	0.09	0.34	0.11
Log MnO	0.900	0.0492	-2.3	-2.4	-2.4	-0.08	0.5
S	0.5933	<0.0001	41	16	16	2.4	6.1
Log S	0.6694	<0.0001	3.3	2.8	2.8	1.35	0.52

decided to substitute the value, for samples returning concentrations equal to this detection limit, with zero. Statistics such as the mean, standard deviation, and threshold values for Cu, Pb, MnO and S are summarized in Table 6.16.

Table 6.16: Threshold values for regolith traverse KP12 (XRF method, n=19).

Element	Mean (M)	Standard deviation (SD)	Threshold values	
			M + SD	M + 2*SD
Cu (ppm)	25	5	30	35
Pb (ppm)	16	3	19	23
MnO (%)	0.10	0.01	0.11	0.12
S (ppm)	30	56	86	142

Zn shows a bimodal distribution (Fig. 6.9 B). The probplot software was used to separate these populations (Fig. 6.10). The observed distribution of Zn (Fig. 6.10) may be ascribed to three sub-populations. The first represents less than 8.6% of the sample population, the second between 8.6% and 64.9% and the third represents 35.1%. The second sub-population is regarded to represent a mixture of the first and third populations. Whereas the first population may reflect the geochemical background, the third population is directly related to the concealed massive sulphide ore zone. The anomalous sub-population of Zn has a threshold value of 112 ppm (Table 6.17).

The outcome of the normality test and the other statistics for Cu, Zn, Pb, MnO, Fe_2O_3 and S concentrations obtained from XRF for regolith traverse T2 in Areachap are summarized in Table 6.18. Based on these results, MnO and Fe_2O_3 display normal distributions, whereas Cu, Zn, Pb and S show lognormal distributions.

Table 6.17: The threshold value of Zn for regolith traverse KP12 (XRF analysis, n=19 samples).

Element	No. of popul.	Means (M)	Std. Dev. (SD)	%	Threshold values
Zn (ppm)	1	89	-86.6 +92	8.7	84 95
	2	98	-92.1 +103.7	56.3	87 110
	3	129	-120 +137.5	35	112 147

Note: No. of popul.: Number of population, SD: Standard deviation

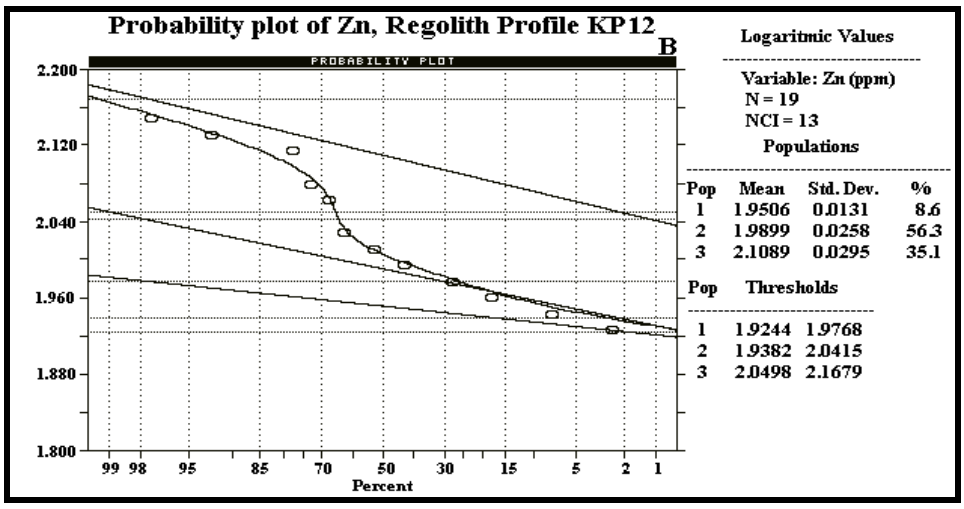

Figure 6.10: Probability plot of Zn based on the regolith traverse KP12 data, Kantienpan, XRF method.

Table 6.18: Results of the normality test for regolith traverse of T2 (XRF method, n = 25).

Element	Shapiro-Wilk		Mean	Median	Mode	Skewness	Kurtosis
	W	Pr<W					
Cu (ppm)	0.7747	<0.0001	38	29	29	1.7	2.5
Log Cu	0.8769	0.0060	3.6	3.4	3.4	1	0.2
Zn (ppm)	0.8030	0.0003	97	84	79	1.3	0.3
Log Zn	0.8689	0.0041	4.5	4.4	4.4	0.9	-0.3
Pb (ppm)	0.6937	<0.0001	25	22	21	2.4	5.6
Log Pb	0.8138	0.0004	3.2	3.1	3	1.7	3
MnO (%)	0.9037	0.0221	0.08	0.08	0.08	0.8	0.8
Log MnO	0.9174	0.0447	-2.6	-2.5	-2.5	0.3	-0.3
Fe_2O_3 (%)	0.9488	0.2350	5.7	5.6	5.6	0.6	-0.02
Log Fe_2O_3	0.9602	0.4193	1.7	1.7	1.7	0.4	-0.2
S (ppm)	0.5758	<0.0001	329	124	69	2.7	7.1
Log S	0.9556	0.3345	5.1	4.8	4.2	0.5	0

The probability graphs of the normal and log values of the elements are given in Figure 6.11. MnO and Fe_2O_3 have single normal distributions and Cu, Pb and S have single lognormal distributions. The statistics including the mean, standard deviation,

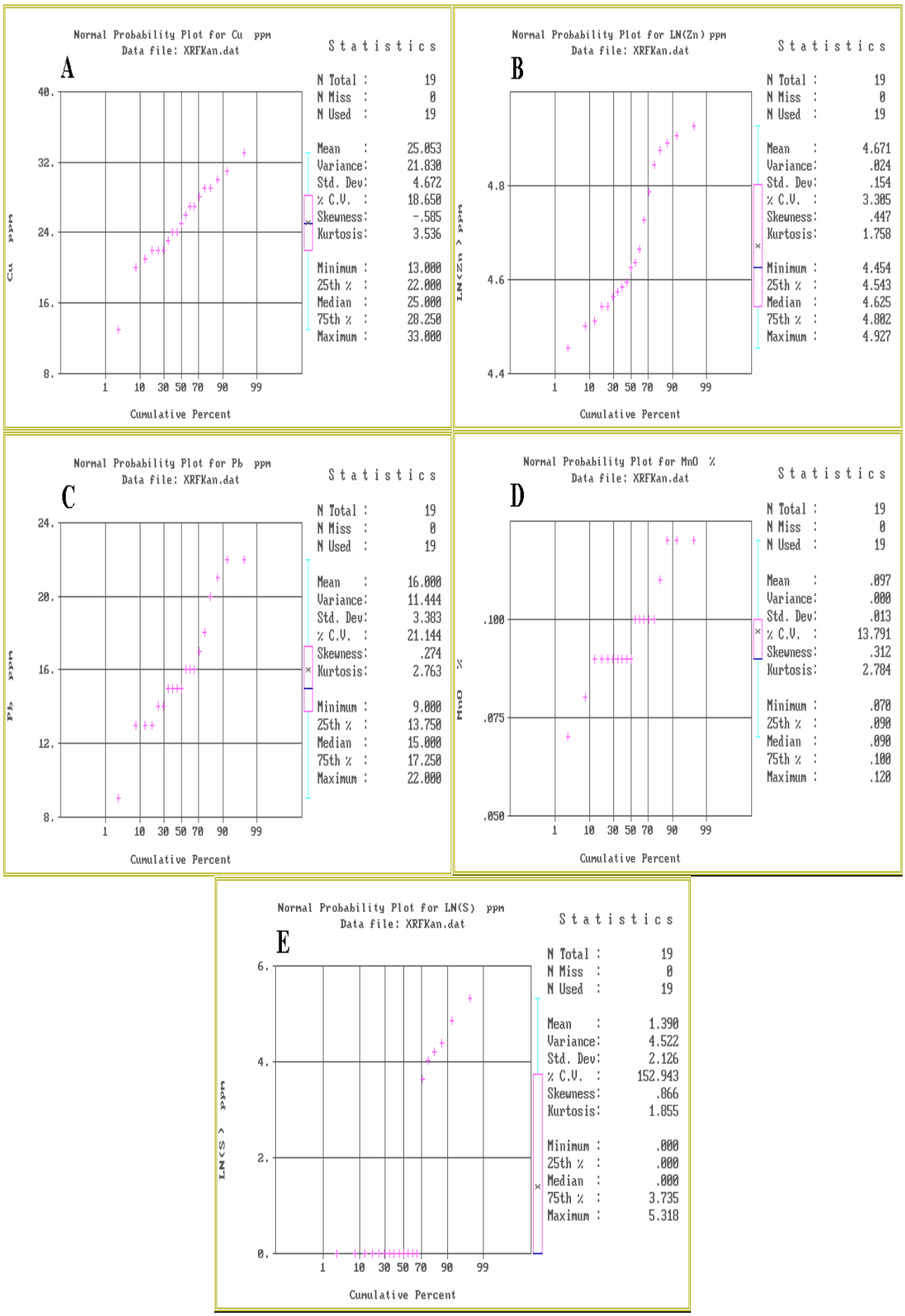

Figure 6.9: Probability plot of the normal and log values for Cu (A), Zn (B), Pb (C), MnO (D) and S (E), regolith traverse KP12, Kantienpan (XRF method, n=19 samples).

and threshold of these elements are summarized in Table 6.19.

Table 6.19: Threshold values for regolith traverse T2 (XRF method, n=25).

Element	Mean (M)	Standard deviation (SD)	Threshold values	
			M + SD	M + 2*SD
Cu (ppm)	38	18	56	74
Pb (ppm)	25	7	32	39
MnO (%)	0.08	0.02	0.1	0.12
Fe_2O_3 (%)	5.69	0.48	6.2	6.7
S (ppm)	329	496	825	1321

Zn shows a bimodal distribution (Figure 6.11 B) and the probplot software was used to separate these populations (Fig. 6.12). The observed distribution of Zn may be considered to be composed of three sub-populations. The first represents less than 66.2% of the sample population, the second between 66.2% and 80.3% and the third represents 19.7%. The second sub-population probably represents a mixture of the first and third. The anomalous sub-population of Zn has a threshold value of 135 ppm (Table 6.20).

Table 6.20: Threshold values for Zn, regolith traverse T2 (XRF method, n=25 samples).

Element	No. of popul.	Means (M)	Std. Dev. (SD)	%	Threshold values
Zn (ppm)	1	77	-68.3 +87.5	66.2	60 99
	2	101	-86.3 +117.4	14.1	74 137
	3	159	-146.8 +172.6	19.7	135 187

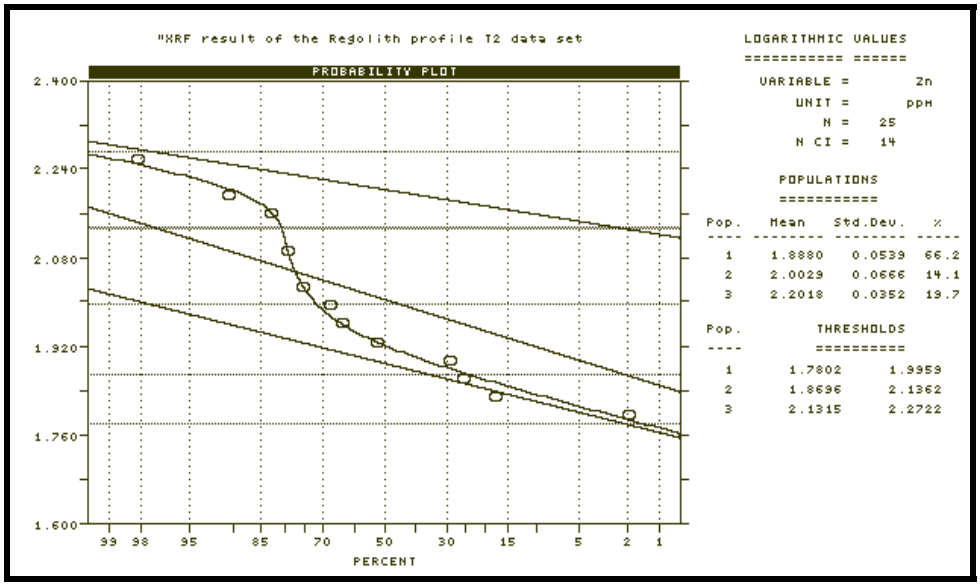

Figure 6.12: Probability plot of Zn, regolith traverse T2 (XRF method, n=25 samples).

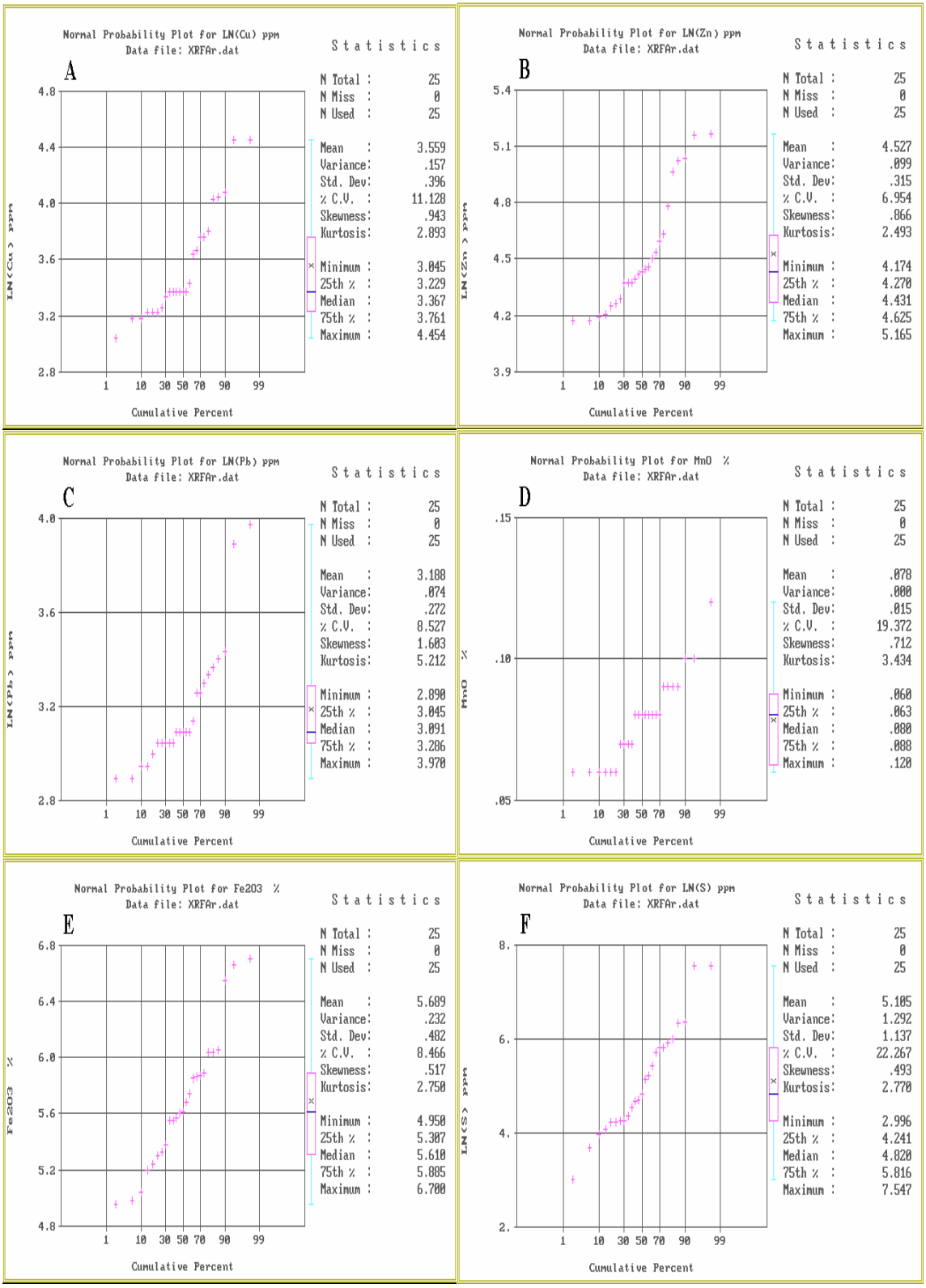

Figure 6.11: Probability plot of the normal and log values for Cu (A), Zn (B), Pb (C), MnO (D), Fe_2O_3 (E) and S (F), regolith traverse T2, Areachap (XRF method, n=21 samples).

6.6. Discrimination of concealed ore zones in the surface samples

The anomalous samples in the regolith traverses in the Kantienpan and Areachap may be identified relative to the threshold values calculated for Cu, Zn, Pb, Mn, MnO and S as analyzed by ICP-MS (for NH_4EDTA and $Ca(H_2PO_4)_2$ solutions) and XRF methods. The threshold values and the traverse background may then be used to determine the width of the secondary dispersion haloes in the studied areas.

6.6.1. Comparison of partial extraction techniques with total analysis method

Traverse KP12 (Kantienpan)

In Figures 6.13 to 6.17 the results of ICP-MS and XRF analyses for each element and oxide are plotted for regolith traverse KP12 at Kantienpan. A cross section which includes the location of regolith samples and the approximate projection of the ore body is also provided. There are two massive sulphide lenses in this cross-section and their projection positions at surface are from 150 to 170 (from sample 9 to 11) and 200 to 220-m (from sample14 to 16). The grade of the ore zones are given in the cross sections (Fig. 6.13 to 6.17).

The ICP-MS results for EDTA soluble Cu (threshold value 5768 ppb, Fig. 6.13 A) are not diagnostic of the underlying mineralization, but there is an increasing trend between 180 and 240 and a peak at 150-m distance. The values are lower than the threshold value, but higher than the traverse background (Fig. 6.13 A). Another peak higher than the traverse background occurs at 0-m, which is located above the quartzo-feldspathic gneiss rocks which have a Cu content of 7 ppm (unit 5 in the cross section, under the calcrete and sand cover). On the other hand, XRF analyses of this element (Fig. 6.13 B) show three anomalous peaks (threshold value 30 ppm) at 150, 180 and 240-m distances. Cu values between 200 and 250-m distance are higher than the traverse background, but lower than the threshold value. Between 80 and 120-m distance, located above the amphibolite rocks (unit 6 in the cross section), there is a peak which is higher than the traverse background (Fig. 6.13 B). The amphibolite contains 4 to 359 ppm Cu.

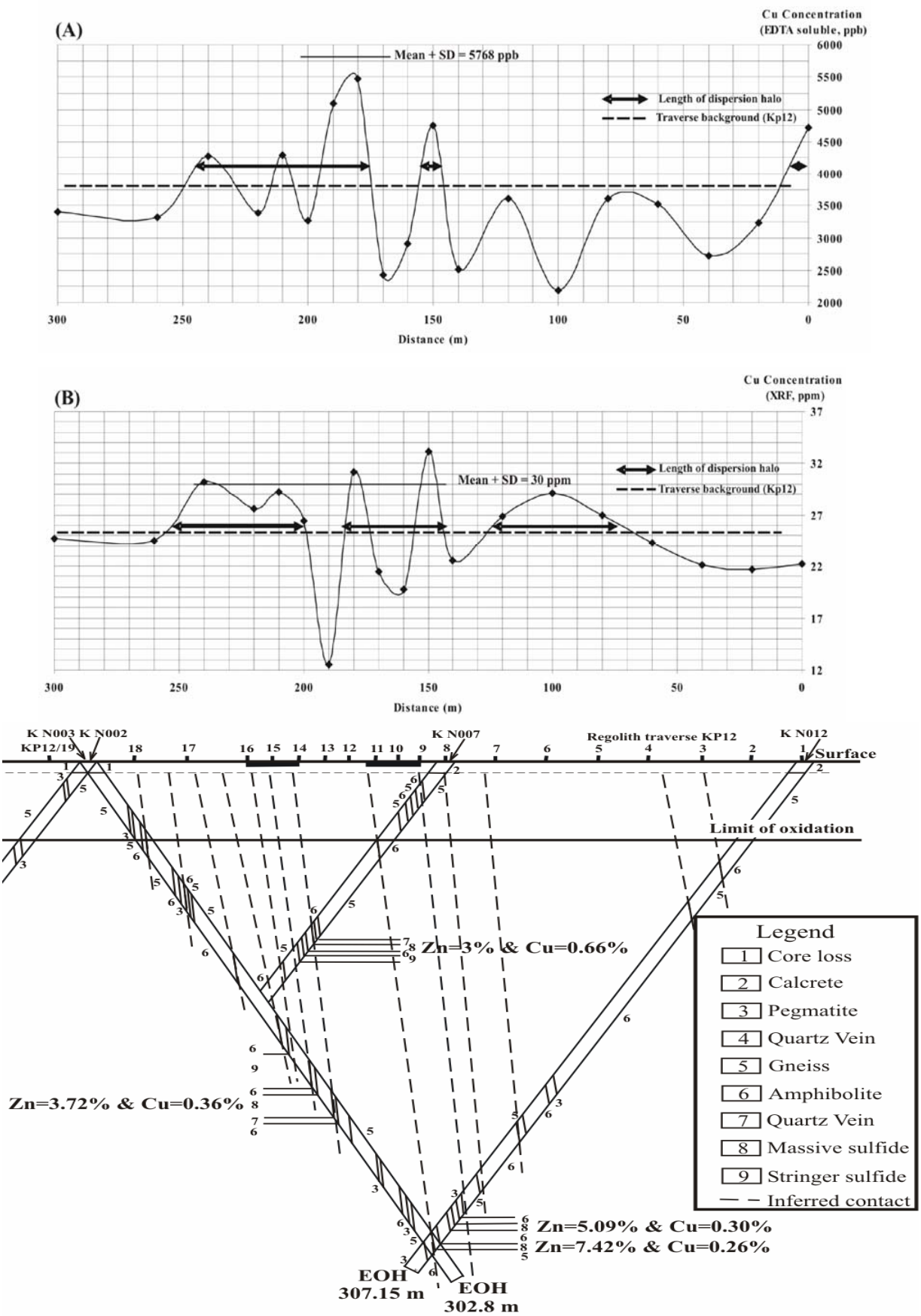

Figure 6.13: Variation of Cu in regolith traverse KP12 based on ICP-MS (A, by using NH_4EDTA and 180-minutes shaking times) and XRF analyses (B).

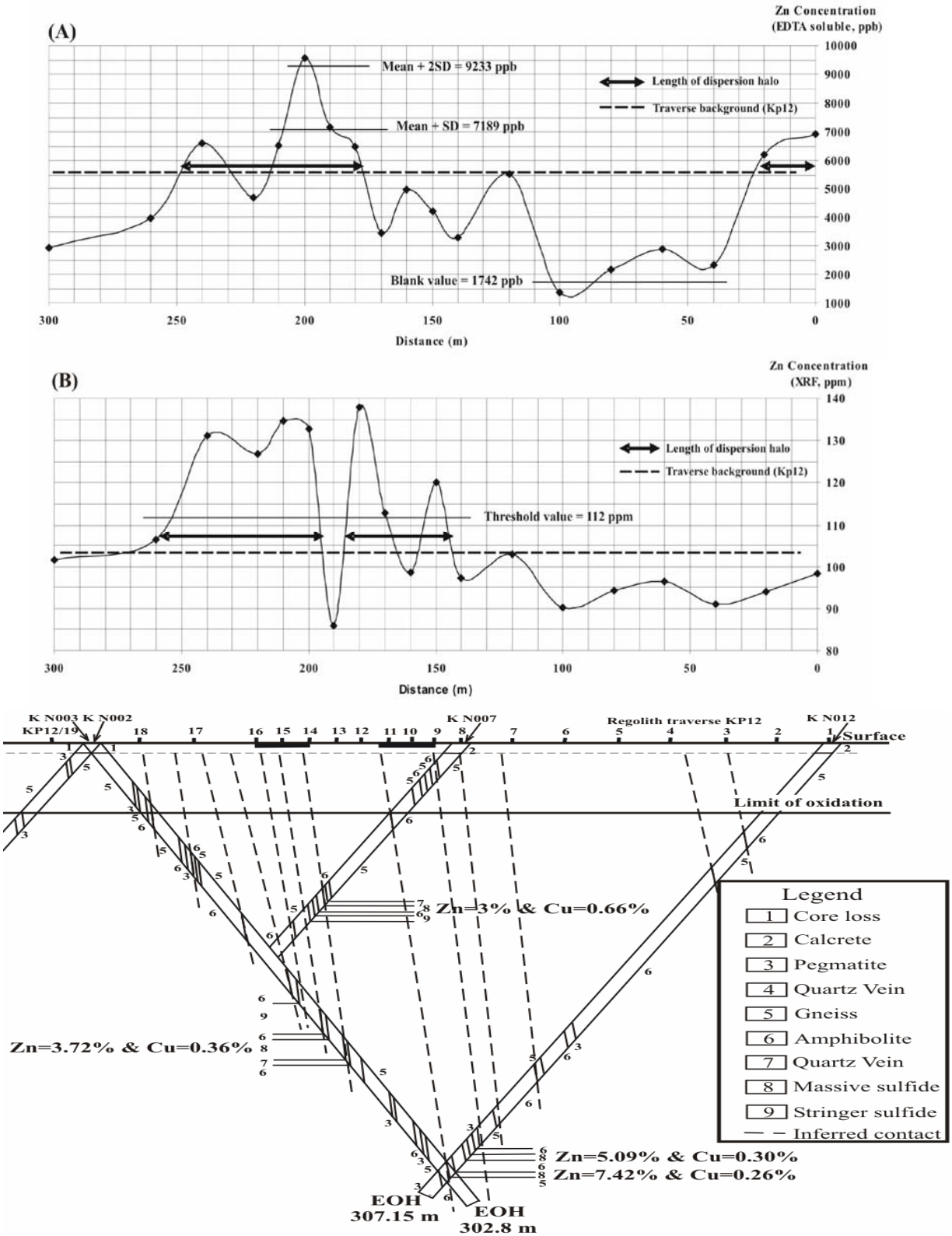

Figure 6.14: Variation of Zn in regolith traverse KP12 based on ICP-MS (A, by using NH_4EDTA and 180-minutes shaking times) and XRF analyses (B).

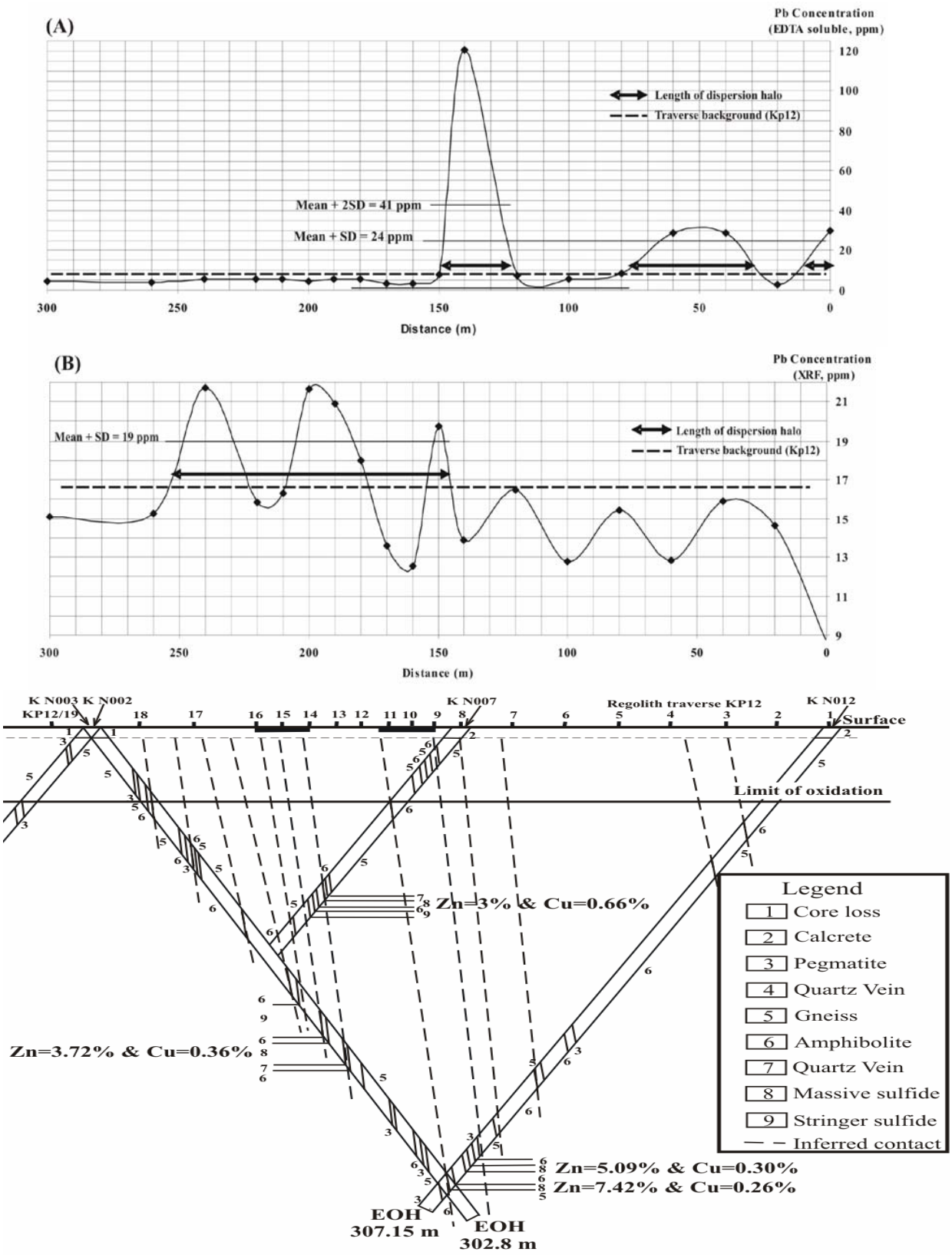

Figure 6.15: Variation of Pb in regolith traverse KP12 based on ICP-MS (A, by using NH_4EDTA and 180-minutes shaking times) and XRF analyses (B).

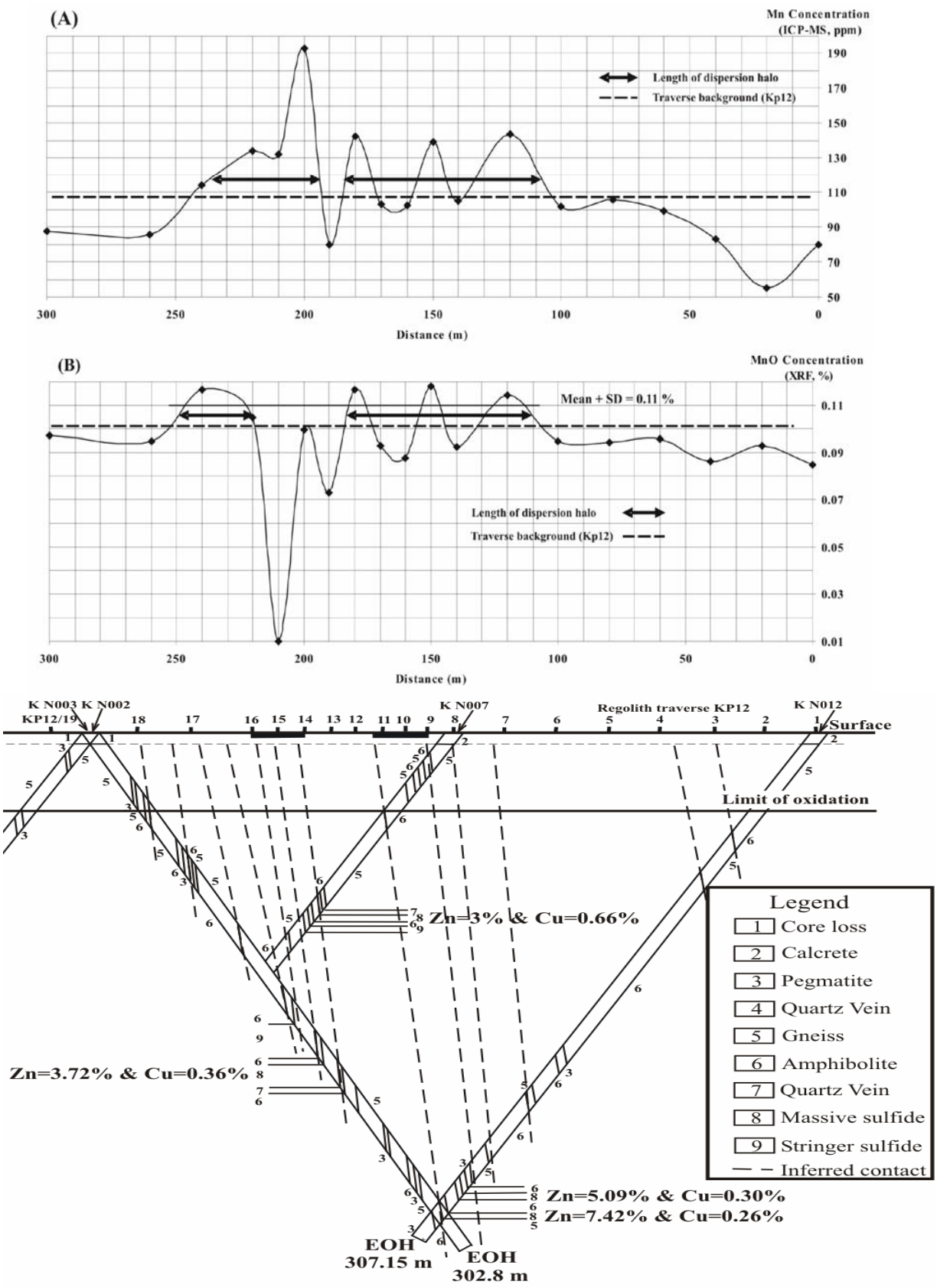

Figure 6.16: Variation of Mn in regolith traverse KP12 based on ICP-MS (A, by using NH_4EDTA and 180-minutes shaking times) and XRF analyses (B).

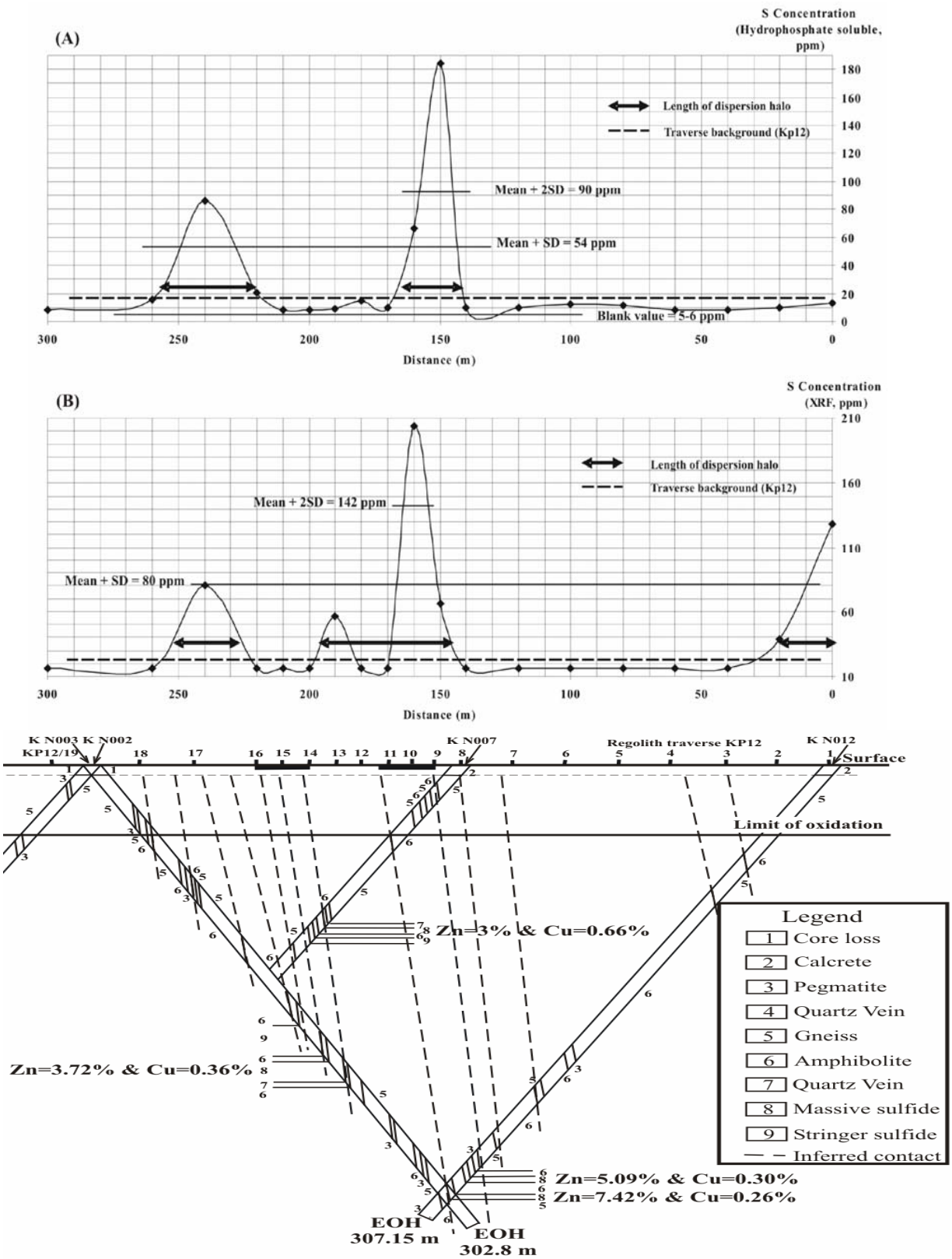

Figure 6.17: Variation of S in regolith traverse KP12 based on ICP-MS (A, by using NH_4EDTA and 180-minutes shaking times) and XRF analyses (B).

The variation of Cu in both methods confirms the existence of two lenses of concealed ore. XRF results show two clear peak areas above the concealed ore, but

the EDTA extraction method shows a narrow sharp peak for one and shows both elevated and low values dispersed over a larger area for the second ore zone. In general, the EDTA extraction and XRF methods display Cu dispersion haloes that have approximately the same width.

Figure 6.14A and 6.14B shows the variation of Zn analysed by ICP-MS and XRF. Based on the threshold value of Zn as determined by ICP-MS (7189 ppb), there is an anomalous peak between 180 and 210-m distance. However, based on the traverse background, ICP-MS results show a peak area from 180 to 250 and a peak between 0 to 20-m distances. Again, the last peak is located above the quartzo-feldspathic rocks (unit 5) where the Zn content is 98 ppm. XRF results (threshold value 112 ppm) also show an anomalous area between 200 and 250 m, and two anomalous peaks at 180 and 150-m distance. If the traverse background is considered for XRF results, then Zn shows two peaks, one from 150 to 180 and the other from 200 to 260-m distance.

The partial extraction method shows only one anomalous area whereas the XRF results show two which are located above the two concealed ore lenses. XRF also shows a wider dispersion halo for Zn in comparison to partial (EDTA) extraction.

Pb (Fig. 6.15 A) displays two anomalous peaks at 0 and 140 m (unit 5), an anomalous area from 40 to 60-m (unit 5 and 6) based on the ICP-MS results (threshold 24 ppm) and traverse background. However, XRF analysis (Fig. 6.15 B, threshold value 19 ppm), display an anomaly between 190 and 200 m and two anomalous peaks at 150 and 240-m distance. Based on the traverse background, there is peak area from 150 to 250-m.

The partial (EDTA) extraction method only shows one narrow peak near one of the ore lenses when projected on surface. The XRF results also show a narrow peak at one of the locations and wider dispersion haloes and thus better identification of the concealed ore lenses than the partial (EDTA) extraction.

Mn analyzed by ICP-MS does not show anomalous values (Fig. 6.16, threshold value 327 ppm). Mn shows a peak area from 110 to 240-m. Four anomalous peaks can be identified based on XRF results of Mn (Fig. 6.16 B) i.e., at 120, 150, 180 and 240-m

distance. Based on the traverse background and threshold value of Mn for XRF results, there are two peak areas, i.e., from 210 to 240 and from 110 to 180-m distance.

Partial (EDTA) extraction and total analyses (XRF) results show the same dispersion halo span for Mn. The XRF results show two separate anomalies for the two concealed ore lenses, but the partial extraction shows an approximately continuous halo based on the traverse background.

S shows anomalous areas for both ICP-MS (threshold value 54 and 90 ppm) and XRF (80 and 142 ppm) analyses between 150 and 160 and at 240-m distances (Fig. 6.17 A and Fig. 6.17 B). XRF results (Fig. 6.17 B) show a third anomalous peak at 0 (unit 5, where the S content is 81 ppm). Based on the traverse background for XRF results, one of the peak areas is from 150 to 200-m.

The sulphur concentration shows anomalous peaks above the concealed ore lenses that are projected to surface, but these haloes are narrower than for the other elements. The XRF results show a slightly wider halo when compared to that of partial (EDTA) extraction for one of the locations.

Based on these observations, Cu, Mn and especially Zn may be used to locate the (residual) anomalous area in the regolith traverse.

Later, for the two other traverses in the Kantienpan (KP5 and KP8), the variation of Cu, Zn and Mn will be discussed based on analytical results from the ICP-MS method.

Traverse T2 (Areachap)

Figures 6.18 to 6.23 show the results of ICP-MS and XRF analyses for Cu, Zn, Pb, Fe_2O_3, MnO and S at Areachap in regolith traverse T2, which crosses over the ore deposit and its host rocks. Also shown in the figures is a cross section showing the location of the regolith samples and the surface projection of the ore zone (from sample 30 to -40 m). In Figure 6.18, the variation of Cu, determined by ICP-MS and XRF, is shown. Based on the threshold value of the ICP-MS for Cu (8339 ppb, Fig.

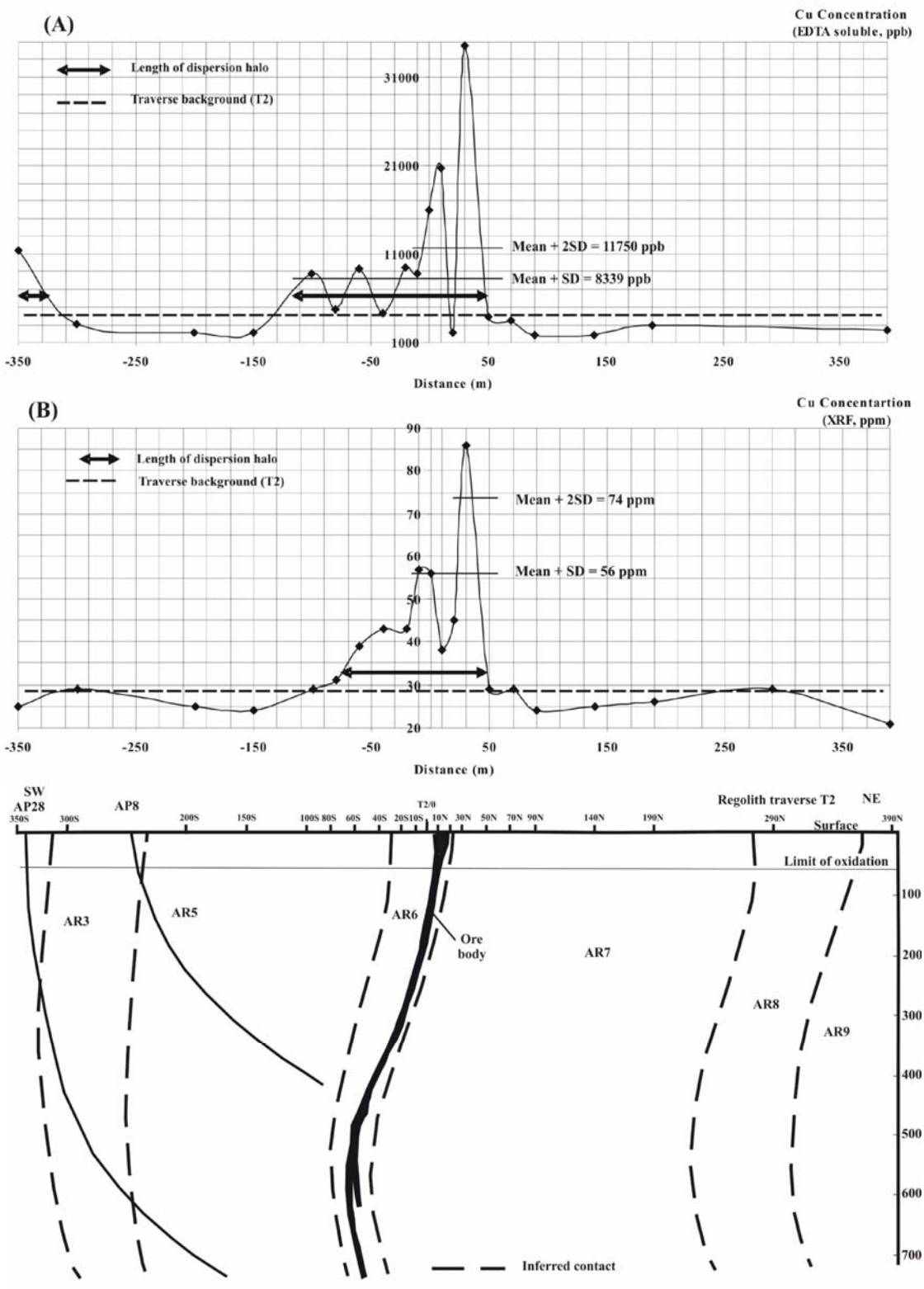

Figure 6.18: Variation of Cu in the regolith traverse T2 based on ICP-MS (A) (NH_4EDTA, 180-minutes shaking times) and XRF (B) analysis.

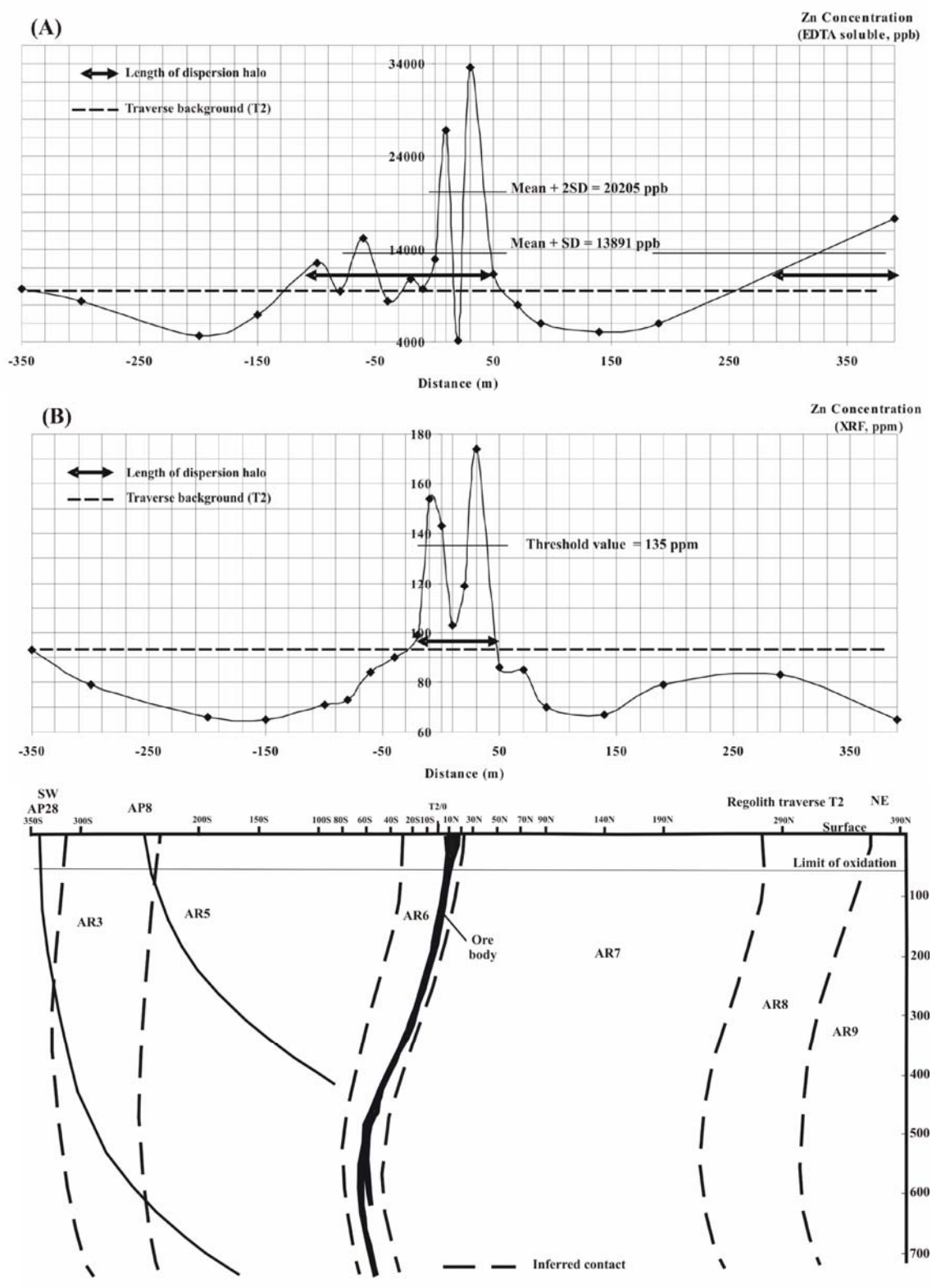

Figure 6.19: Variation of Zn in the regolith traverse T2 based on ICP-MS (A) (NH_4EDTA, 180-minutes shaking times) and XRF (B) analysis.

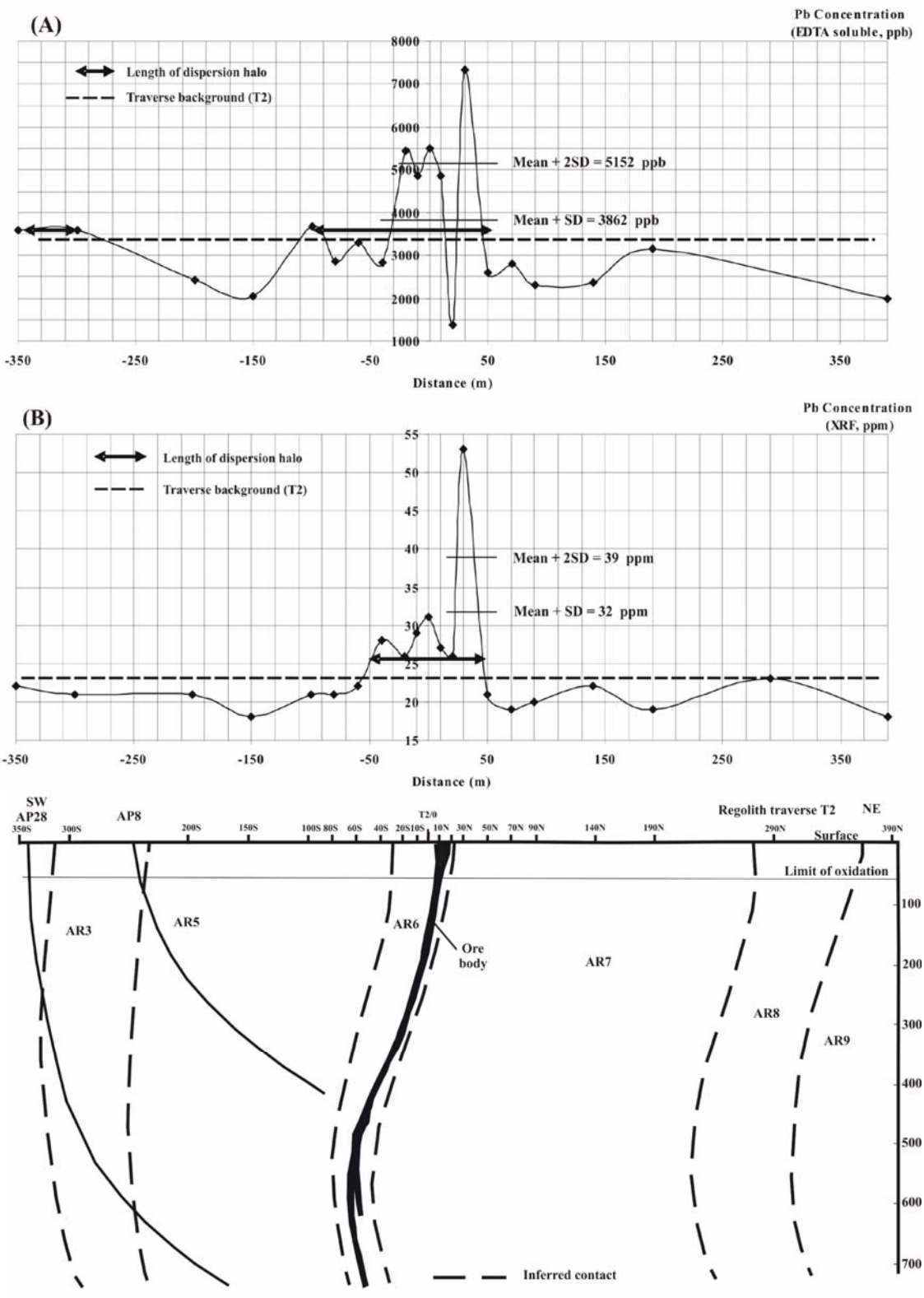

Figure 6.20: Variation of Pb in the regolith traverse T2 based on ICP-MS (A) (NH_4EDTA, 180-minutes shaking times) and XRF (B) analysis.

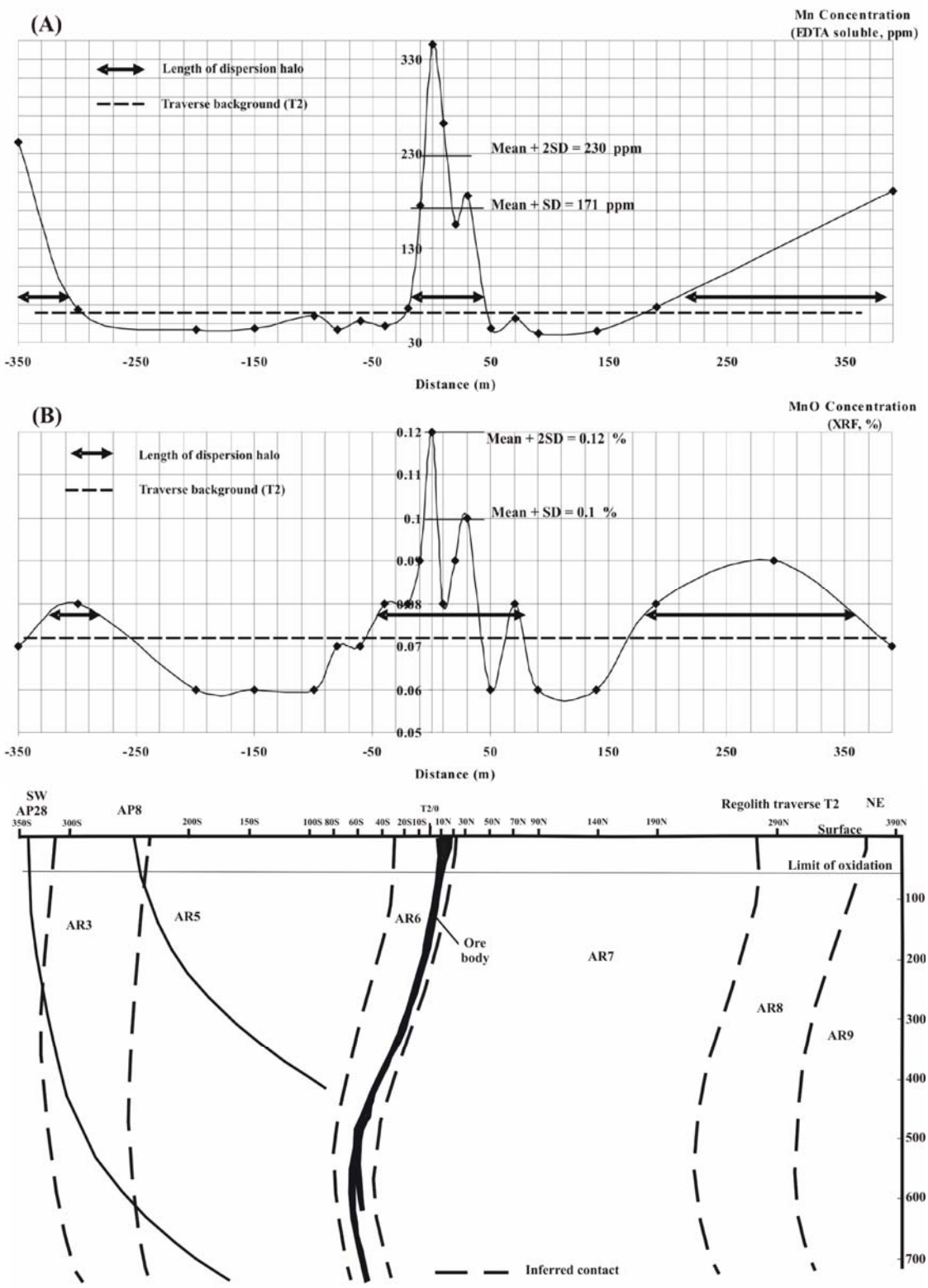

Figure 6.21: Variation of Mn in the regolith traverse T2 based on ICP-MS (A) (NH_4EDTA, 180-minutes shaking times) and XRF (B) analysis.

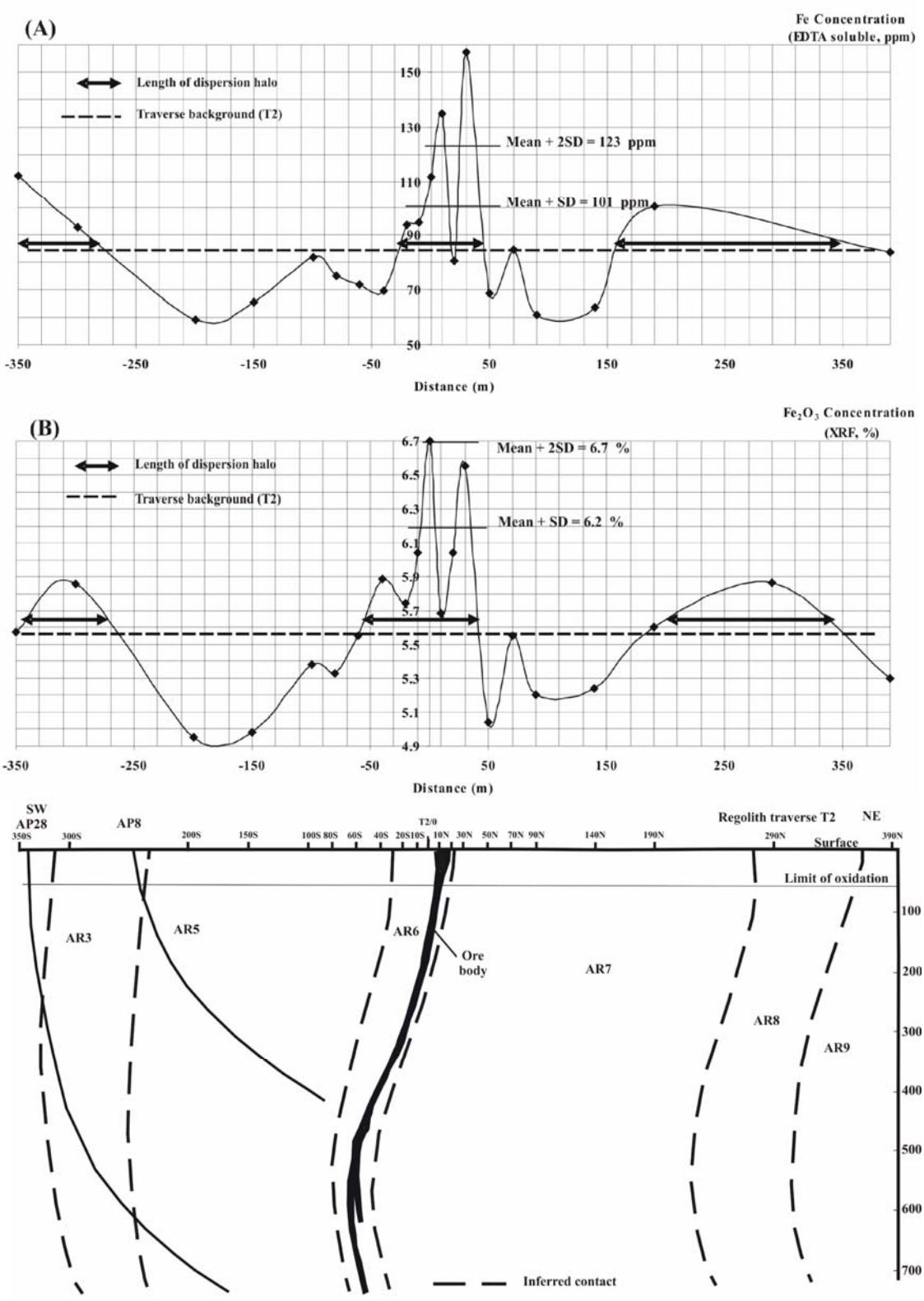

Figure 6.22: Variation of Fe in the regolith traverse T2 based on ICP-MS (A) (NH_4EDTA, 180-minutes shaking times) and XRF (B) analysis.

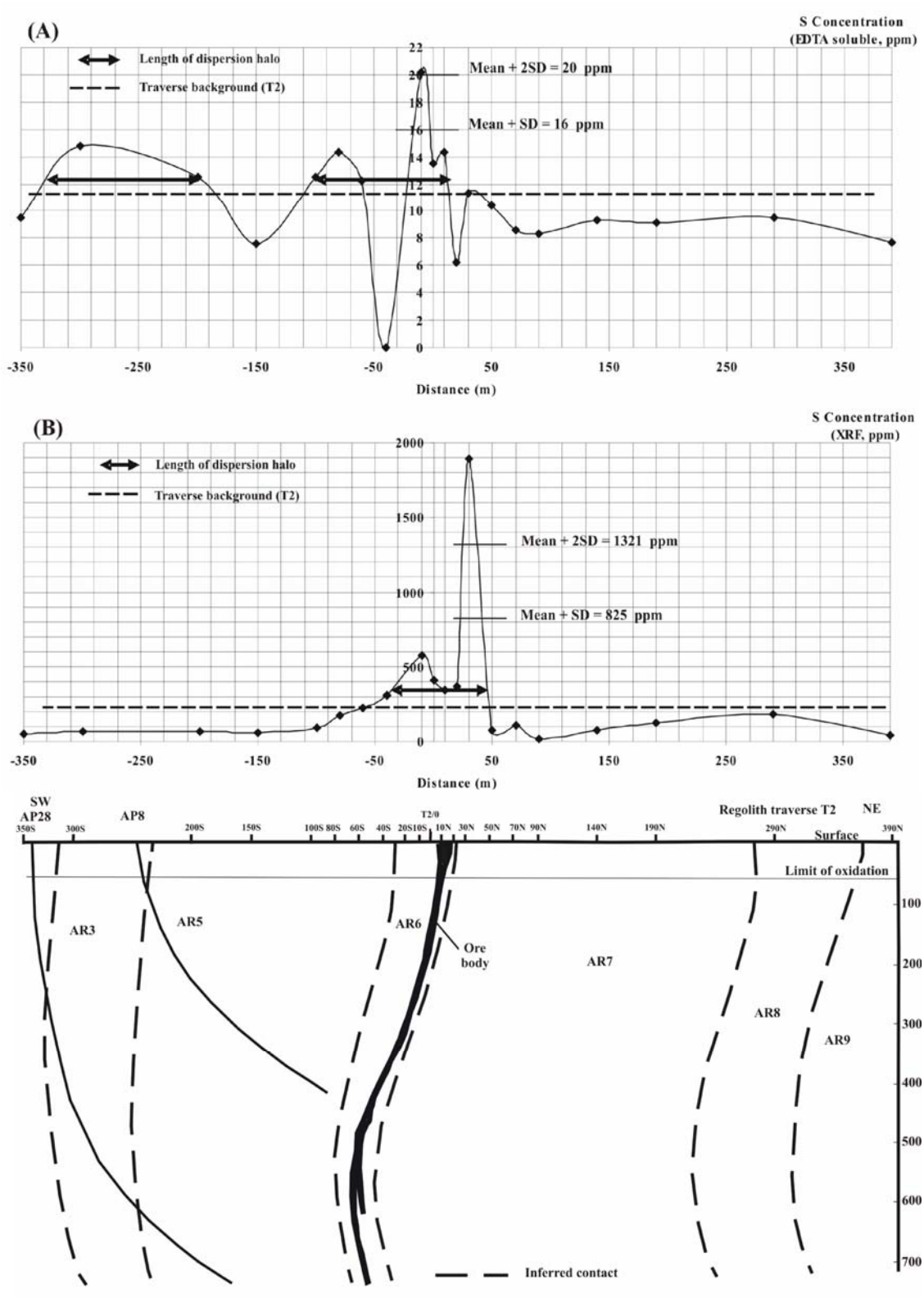

Figure 6.23: Variation of S in the regolith traverse T2 based on ICP-MS (A) (NH_4EDTA, 180-minutes shaking times) and XRF (B) analysis.

6.18 A), there is an anomalous zone from -110 to 50 m. XRF results for Cu (threshold value 56 ppm, Fig. 6.18 B) show an anomalous zone from -10 to 40 m, coinciding

with the expected locations of the ore body host rocks (AR6 symbol in the cross section) under the calcrete and sand cover. Based on the traverse background, peaks occur from -120 to 50 and -70 to 50-m distance for ICP-MS and XRF results, respectively.

The partial (EDTA) extraction of Cu shows wider dispersion haloes when compared to the XRF analyses.

The variation of Zn for ICP-MS and XRF results is shown in Figure 6.19. Based on the Zn threshold value as determined by ICP-MS (13891 ppb), there are two anomalous peaks at 0 and 30 m, which are located directly above the mineralized rocks and a third at 390 m, located at the right end of this traverse. The latter peak is related to the banded pelitic gneiss (unit AR8 in the cross section). This unit may be a metasedimentary rock with a higher Zn background content. The ICP-MS results show another anomalous peak at -60 m, which may be assumed to be part of the mineralized zone. XRF results of Zn show two anomalous peaks (135 ppm) from -10 to 0 and at 30 m, nearly at the same location as the ICP-MS results. Based on traverse background, peak values in T2 occur from -110 to 50 and -20 to 50 m for ICP-MS and XRF results, respectively.

The partial (EDTA) extraction of Zn shows a wider dispersion halo when compared to that of the total analyses (XRF), a trend similar to that shown by Cu.

Figure 6.20 shows the variations of Pb as determined by ICP-MS and XRF results. With a threshold value of 3862 ppb for Pb (Fig. 6.20 A), an anomalous zone from -30 to nearly 50 m has been identified. The XRF results of Pb only show a peak at 30 m. Based on traverse background of T2, peaks occur from -110 to 50 and -50 to 50 m distance for ICP-MS and XRF results, respectively.

The partial (EDTA) extraction of Pb shows wider dispersion haloes in comparison to the total analyses (XRF), as noted in the Cu and Zn dispersion haloes.

The variation of Mn for ICP-MS and XRF results is shown in Figure 6.21. Based on the threshold value of Mn from ICP-MS (171 ppm, Fig. 6.21 A), there is an anomalous area from -10 to 30 m above the host rock. Samples at either end of this

traverse also show anomalous values for ICP-MS analyses. Samples on the left end side of this traverse occur above the banded garnet-biotite-gneiss (unit AR3 in the cross section) whereas those on the right end of the traverse occur above the biotite-hornblende-gneiss rock (unit AR7), and banded pelitic gneiss rocks (unit AR8, as explained). The gneisses may be sedimentary in origin, possibly explaining the higher Mn background values. XRF results of Mn (threshold value of 0.1%, Fig. 6.21B) show an anomalous area from -10 to 30 m distance. Based on the background values for traverse T2, peaks occur from -20 to 50 and -50 to 40 m for ICP-MS and XRF results, respectively.

The total analyses (XRF) of Mn show a wider dispersion halo when compared to that of the partial (EDTA) extraction.

Figure 6.22 shows the variation in the Fe contents as determined by ICP-MS and XRF results. Based on the threshold value of Fe (ICP-MS data; 101 ppm, Fig. 6.22 A), there is an anomalous zone from -10 to 40 m. Samples at both ends of this traverse (at -350 and 190 m) also show anomalous values for ICP-MS analyses which may be explained as above. XRF results of Fe (threshold value 6.2 %, Fig. 6.22 B) show a small anomalous zone between 0 and 30 m above the ore zone. Based on the traverse background for XRF results, there are two peaks at -350 and 190 m, which are confirming the ICP-MS analyses. In traverse T2, peaks occur from -30 to 50 and -50 to 50 m distance for ICP-MS and XRF results, respectively, based on the background values.

The total analysis (XRF) of Fe shows a wider dispersion halo when compared to that of partial (EDTA) extraction, which is the same as for Mn dispersion haloes.

In Figure 6.23, the variation in S is shown for ICP-MS and XRF results. The threshold value of the S concentrations determined by ICP-MS is 16 ppm (Fig. 6.23 A). An anomalous peak is present at -10 m. The XRF results have a threshold value 825 ppm (Fig. 6.23 B) and show an anomalous peak at 30 m. Based on traverse background values in traverse T2, there are peaks from -90 to 10 m for ICP-MS and from -30 to 50 m distance for XRF results. There is another peak area from -200 to -300 for ICP-MS analyses located above unit AR3.

The partial (EDTA) extraction of S shows wider dispersion haloes when compared to those of the total analyses (XRF), as seen in the Cu, Zn and Pb dispersion haloes.

Elements such as Cu, Zn and Pb show a wider secondary dispersion halo in the ICP-MS results, with Cu and Zn giving the widest halo. Mn and Fe show a slightly wider halo for elements analyzed by XRF and the span of dispersion halo for S analyzed by ICP-MS method is slightly wider than XRF results. Mn, Cu, Zn and Pb variations are also investigated in other traverses (T1 and T3) in the Areachap area.

6.6.2. Discrimination of the secondary dispersion haloes in other traverses

The potentially mobile metal ions of interest (Cu, Zn and Mn) in samples from regolith traverse KP5 were extracted by NH_4EDTA solution and analyzed by ICP-MS. The variation in the concentration of these elements along the traverse is shown in Figures 6.24 and 6.25. The cross section of this traverse, which includes the location of samples and projection of the ore zone on the surface (from 70 to 90 m) are also provided. Based on the calculated threshold values (Cu=5768 ppb, Zn=7189 and 9233 ppb and Mn=327 ppm), all elements show an anomalous peak in concentration at 80 m distance (i.e., from sample 5 to 7). Mn shows additional anomalous peak at 220 m distance. Based on the traverse background (dash line), all elements show an anomaly at 220 or after 200 m, above the amphibolite rocks (unit 6 in the cross section, below the calcrete). This rock contains 4 to 359 ppm Cu, 73 to 112 ppm Zn and 0.09 to 0.24 % MnO contents. Cu contents are only slightly higher than the traverse background at 0 m above unit 3 (pegmatite).

Anomalous concentrations of Cu, Zn and Mn may be used to locate the ore zone. The secondary dispersion haloes of Cu and Zn around the ore zone are wider than that of Mn in this regolith traverse.

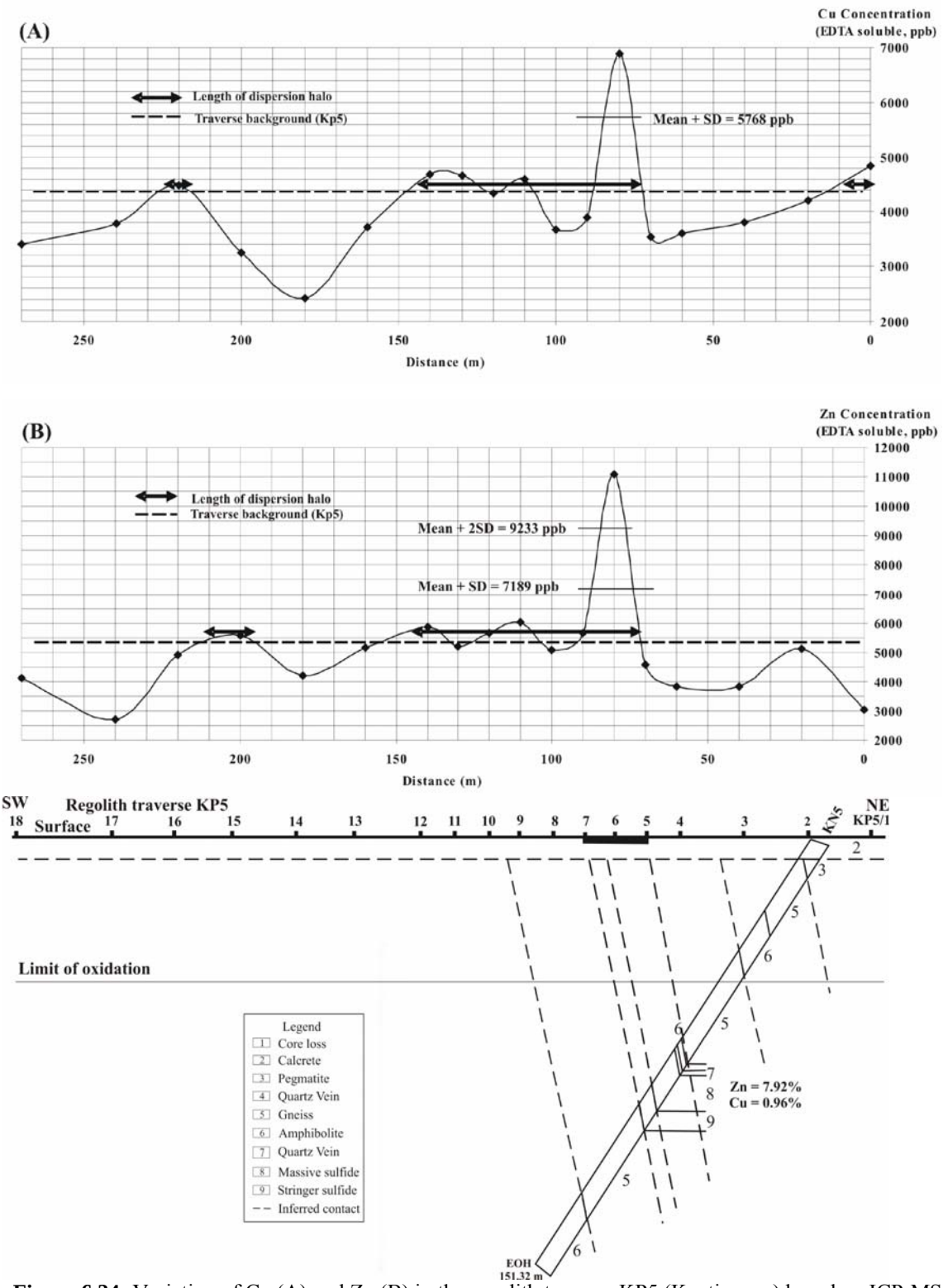

Figure 6.24: Variation of Cu (A) and Zn (B) in the regolith traverse KP5 (Kantienpan) based on ICP-MS analysis (using NH_4EDTA and 180-minutes shaking times).

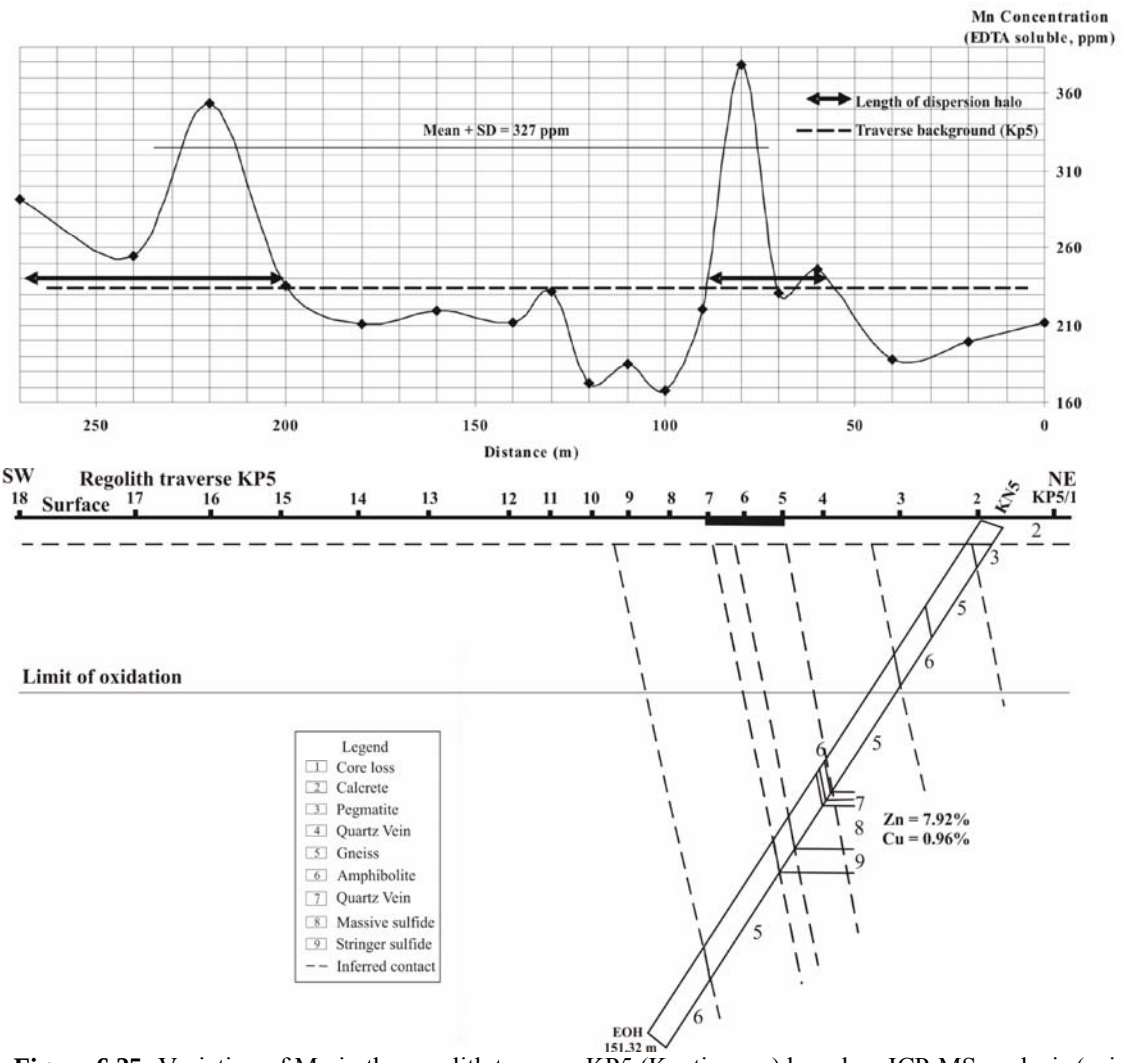

Figure 6.25: Variation of Mn in the regolith traverse KP5 (Kantienpan) based on ICP-MS analysis (using NH_4EDTA and 180-minutes shaking times).

The variations of the mobile metal ions Cu, Zn and Mn, extracted with a NH_4EDTA solution and analyzed by ICP-MS, from traverse KP8 are shown in Figures 6.26 and 6.27. The figure also shows the sample locations, projection of ore zone at surface (at 80, 120 and 170-180 m) and a cross section of the traverse. Based on the calculated threshold values, an anomalous area have been detected from 30 to 140 m that corresponds with the projection of the ore zone. Mn shows another anomalous area from 190 to 270 m, above the weathered amphibolite rocks with Mn contents from 0.09 to 0.24 % (unit 6 in the cross section). Based on the traverse background, the dispersion haloes are slightly wider.

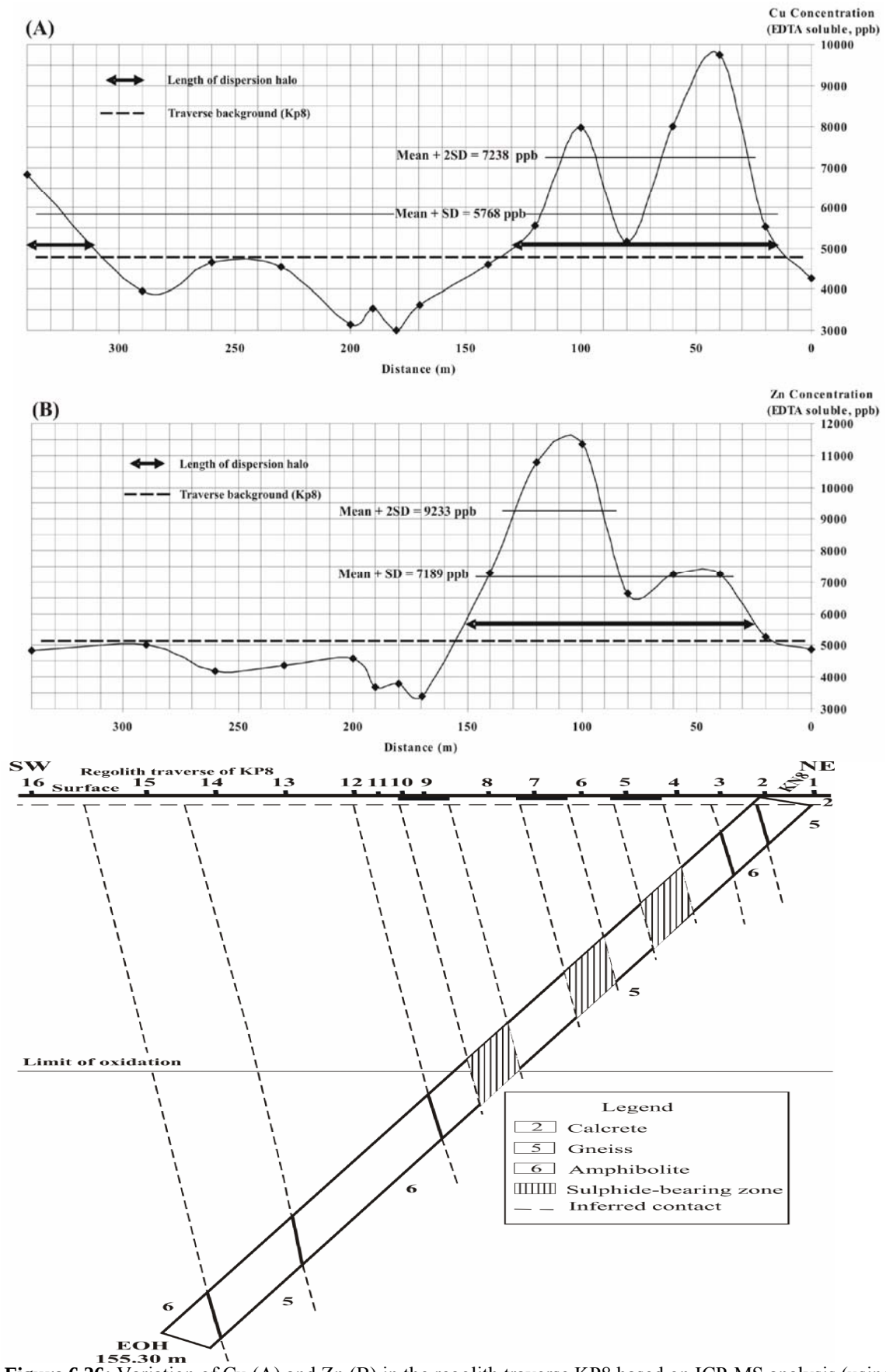

Figure 6.26: Variation of Cu (A) and Zn (B) in the regolith traverse KP8 based on ICP-MS analysis (using NH_4EDTA solutions and 180-minutes shaking times).

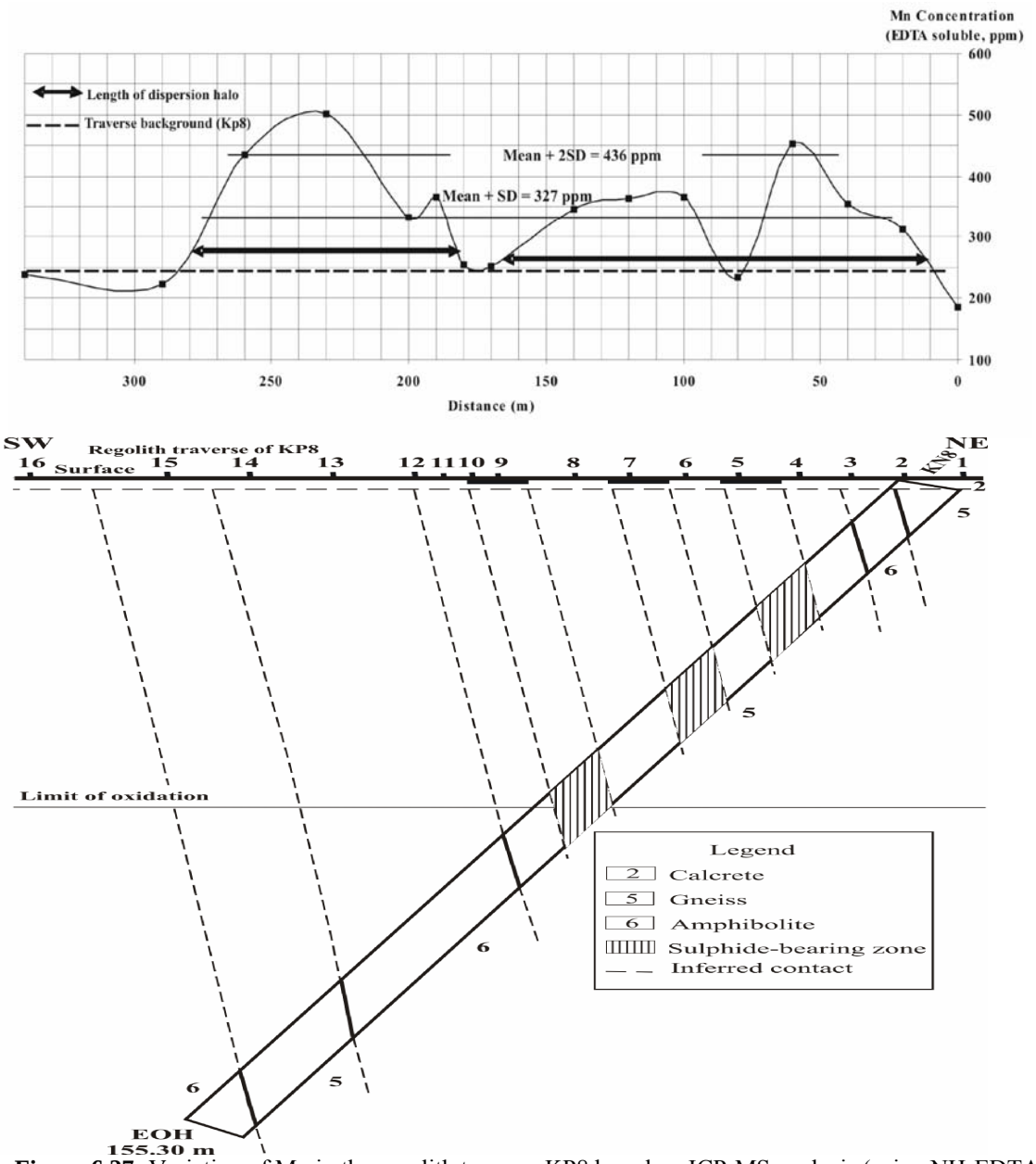

Figure 6.27: Variation of Mn in the regolith traverse KP8 based on ICP-MS analysis (using NH_4EDTA solutions and 180-minutes shaking times).

The ore zone's location at surface is clearly defined by the Cu, Zn and Mn concentrations determined from the NH_4EDTA solution by ICP-MS analyses.

Results of ICP-MS analyses of the extractable Cu, Zn, Pb and Mn concentrations in the regolith traverse T1 at Areachap, located slightly further away from the ore zone, are shown in Figures 6.28 and 6.29. The cross section shows the location of regolith samples and the nature of the underlying geology. Based on the calculated threshold value for Cu (8339 ppb, Figure 6.28 A), there are no anomalous samples, but based

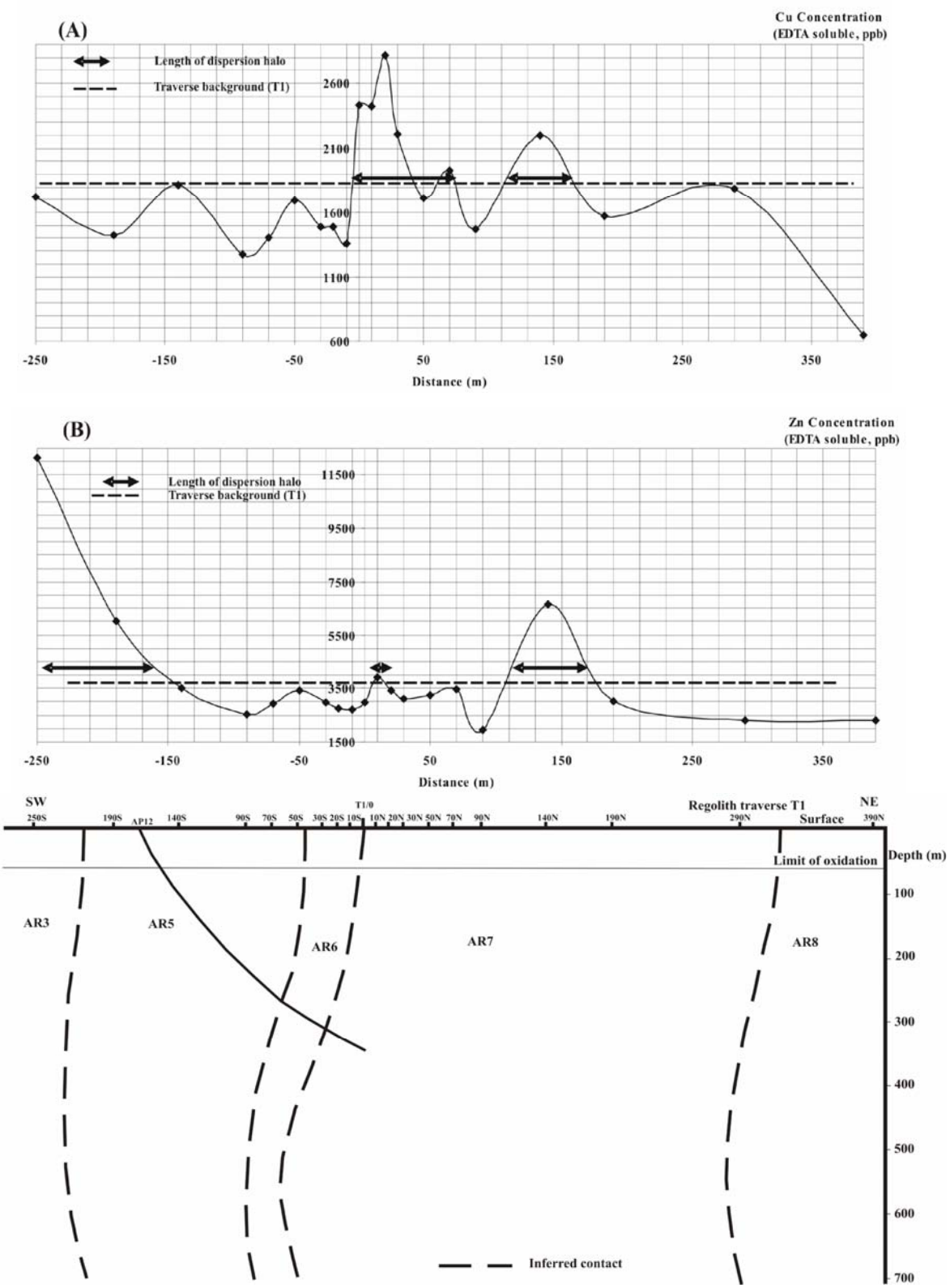

Figure 6.28: Variation of Cu (A) and Zn (B) in the regolith traverse T1 based on ICP-MS analysis (NH_4EDTA, 180-minutes shaking times).

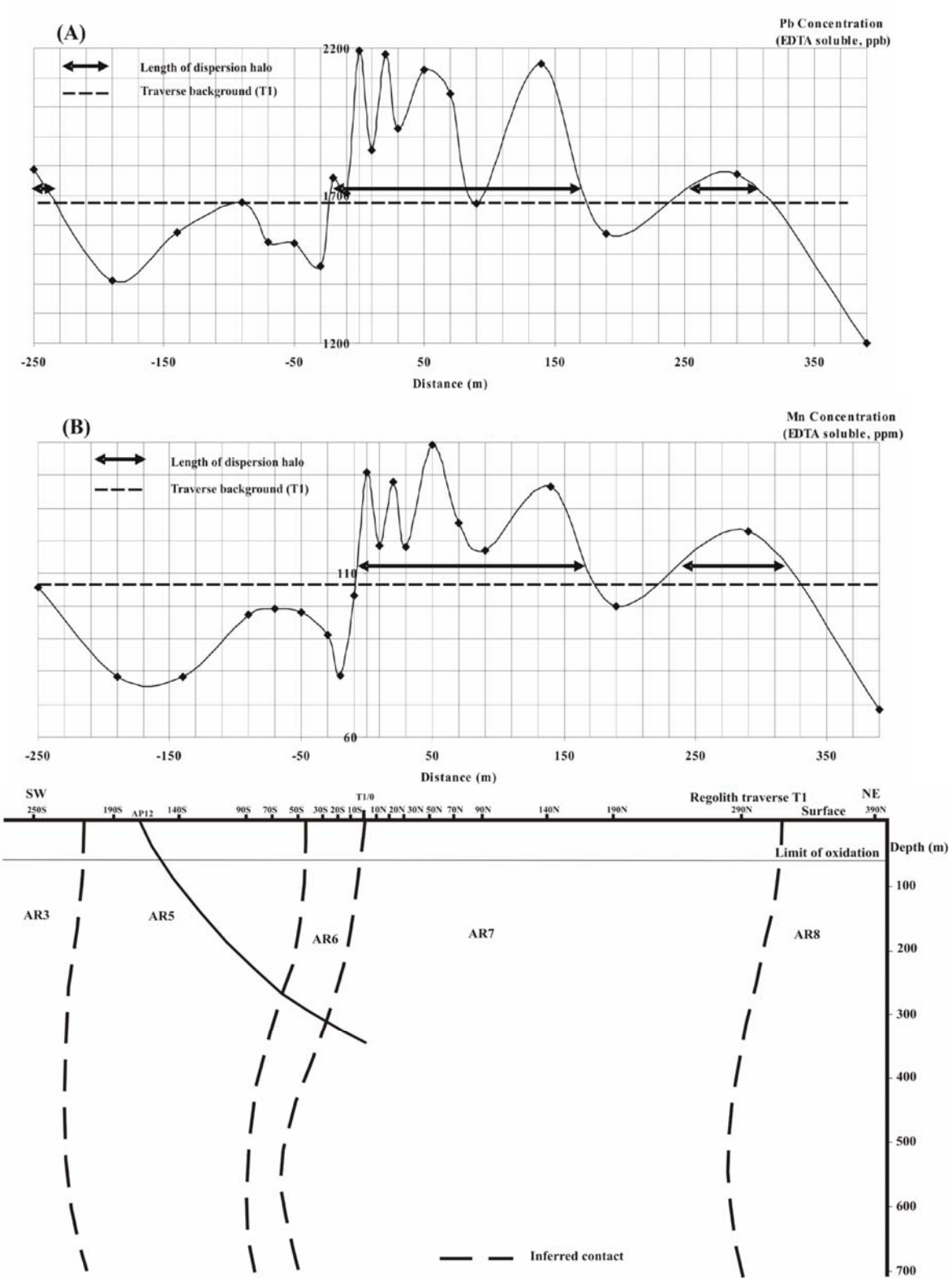

Figure 6.29: Variation of Pb (A) and Mn (B) in the regolith traverse T1 based on ICP-MS analysis (NH_4EDTA, 180-minutes shaking times).

on the traverse background values there is a peak from 0 to 70 m distance above the host rocks. Another peak occurs at 140 m, above the biotite-hornblende-gneiss which has a whole rock Cu concentration of 779 ppm (unit AR7; Theart, 1985).

In Figure 6.28 B, the variation of Zn is shown, with a calculated threshold value of 13891 ppb. No anomaly could be identified above the ore zone (AR6). Zn contents increase from 2000 to 6000 ppb at 140 m (unit AR7 with Zn contents from 5 to 446 ppm), and to 12134 ppb at -250 m (unit AR3, with Zn content 76 ppm).

The variation of Pb is shown in Figure 6.29 A. The calculated threshold value is 3862 ppb Pb. No anomalous sample was identified. Based on the traverse background value, two peaks occur from -20 to 170 and at 290 m, located above the biotite-hornblende-gneiss rock with a whole rock Pb concentration varying from 8 to 47 ppm (unit AR7; Theart, 1985).

Figure 6.29 B shows the variation in Mn with a calculated threshold value of 171 ppm. No anomalous samples were identified. Based on the traverse background value, Mn contents show two peaks, one from -10 to 170 and the other at 290 m distance. These are peaks above the biotite-hornblende-gneiss rock (unit AR7) that may be a metasedimentary rock.

Based on the information available (Voet and King, 1986), this traverse was designed to sample the regolith above the host rock unit (AR6), away from the ore zone in a NE-SW direction. The element concentrations are lower than the anomalous values, and they only show an increasing trend above the stratigraphic extension of the host rock lithology.

Figure 6.30 and 6.31 show variation in the results of ICP-MS determinations of the following elements Cu, Zn, Pb and Mn from the regolith traverse T3, located between traverses T1 and T2. Sample 0 is T1/0 and sample 240 is T2/0 and the traverse overlies the host rock unit (AR6). Borehole AP8 cuts through the ore zone and the projection of the ore zone at the surface is located near the end of this traverse. The locations of regolith samples are also indicated on the cross section. In Figure 6.30, the variation in the concentration of Cu and Zn are shown for ICP-MS results. Based on the calculated threshold value of Cu (8339 ppb, Fig. 6.30 A) there are an anomalous area from 180 to 240 m. Based on the local background for Zn (5000 ppb) in traverse T3 (Fig. 6.30 B) there is an increasing trend in the Zn concentration from 160-m to the end of the traverse.

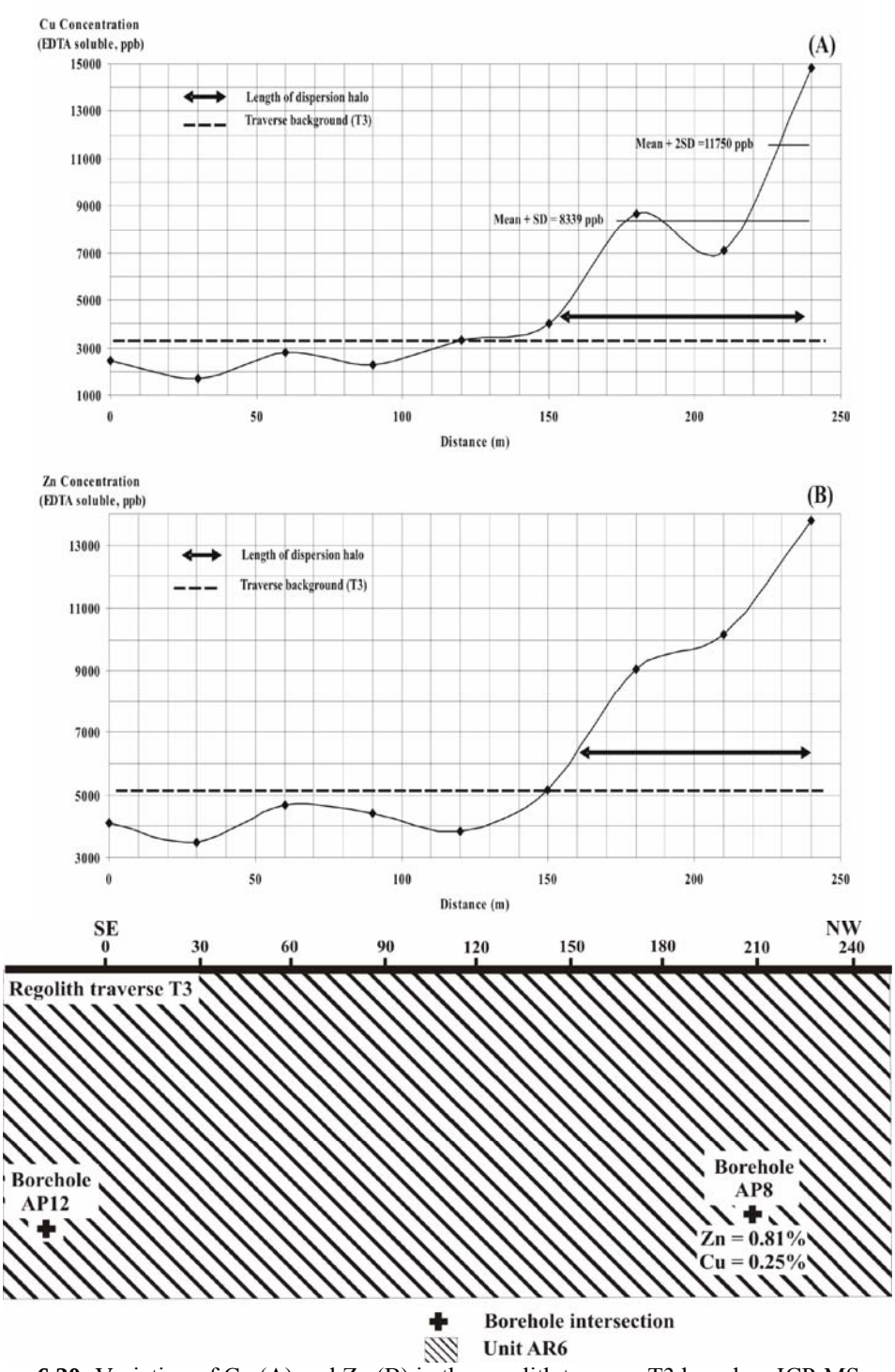

Figure 6.30: Variation of Cu (A) and Zn (B) in the regolith traverse T3 based on ICP-MS analysis (NH_4EDTA, 180-minutes shaking times).

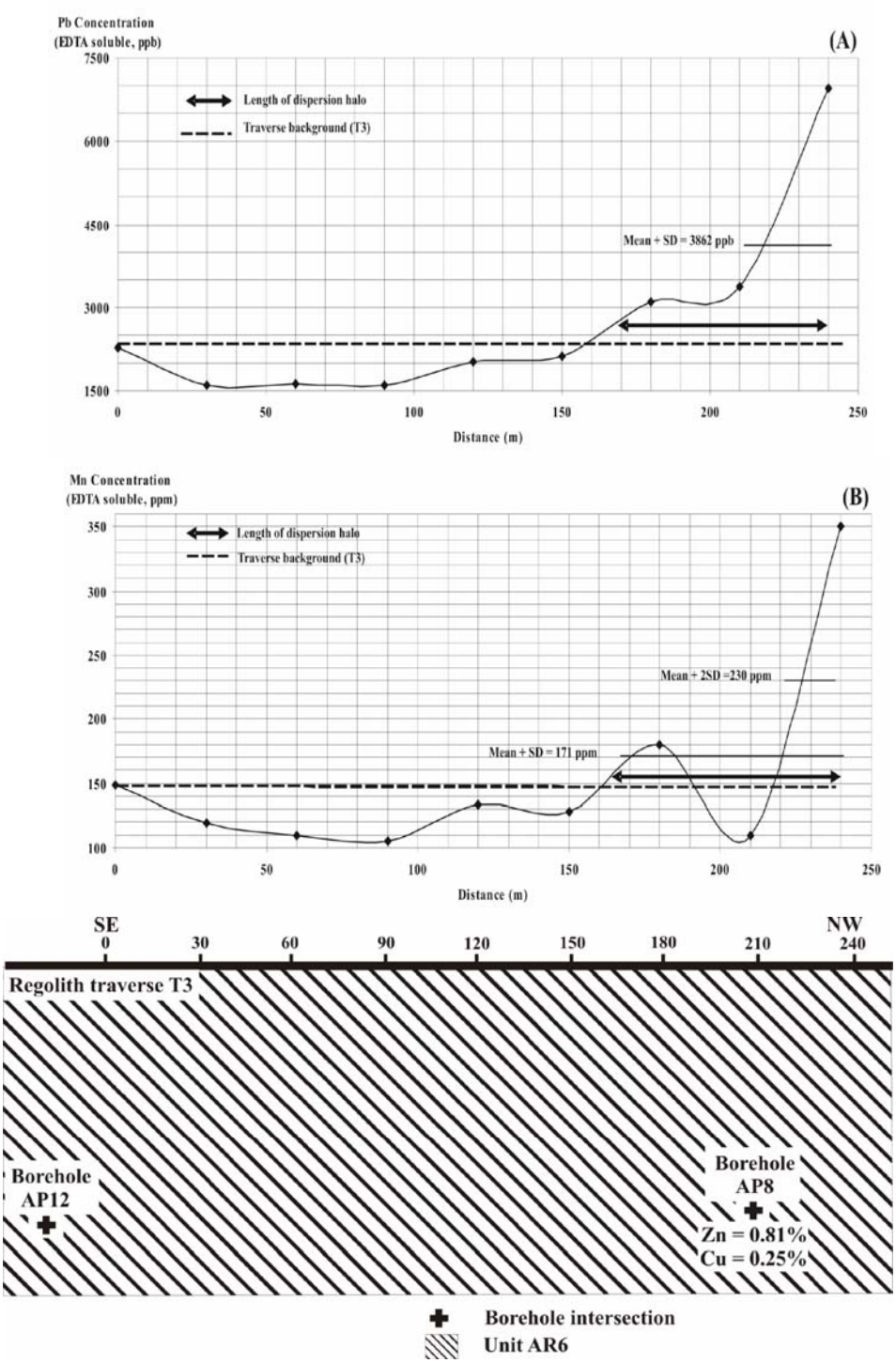

Figure 6.31: Variation of Pb (A) and Mn (B) in the regolith traverse T3 based on ICP-MS analysis (NH_4EDTA, 180-minutes shaking times).

Pb contents are anomalous in samples from 220 to 240 m (calculated threshold value 3862 ppb, Fig. 6.31 A) and Mn contents (calculated threshold value 171 ppm, Fig. 6.31 B) from 170 to 240 m. Based on the traverse background, the peak area extends from 160 to the ore zone at 240 m for both Pb and Mn.

Variations of all elements show an increasing trend and anomalous values towards the ore zone at the end of the traverse. This corresponds to a dispersion halo in this direction of approximately 70 m.

6.6.3. Discrimination of the secondary dispersion haloes (MMI results, Kantienpan)

The variations in the concentration of Cu and Zn in samples from the regolith traverse 7800NW are plotted in Figure 6.32. As this regolith traverse is close to the cross section of KN11 (Fig. 6.3), the profile derived from this drill hole will be used for the interpretation. Cu shows anomalous values from 1200 to 1225 m. Zn values are anomalous from 1100 to 1250 m. Based on the traverse background, this anomaly starts from 1300 m.

The secondary dispersion haloes of these two elements are coincident. Zn shows a wider halo when compared to Cu, as could be expected because of the higher known mobility of Zn in the secondary environment.

Figure 6.33 shows the variation of Cu and Zn concentrations of samples from the regolith traverse 7700NW. Due to the proximity of this regolith traverse to drill hole KN5 (Fig. 6.3), the profile derived from this drill hole will be used for the interpretation. It can be seen that Cu shows five anomalous peaks at 1100 m, 1175 m, 1250 m, 1300 m and 1425 m. Zn shows a very sharp anomalous peak at 1225 m. Based on the traverse background, elevated values start from 1225 and ends at 1350 m. There is another small peak in the Zn concentrations towards the left end of this traverse, located above the weathered amphibolite rocks with 4 to 359 ppm Cu in the whole rock samples (unit 6 in the cross section).

The sinuous nature of the variation in Cu concentrations makes it difficult to distinguish the exact location of the anomaly. Zn variation defines a better anomalous zone above the assumed projection of the ore deposit.

Taking these results into account the variation in Zn concentration is better suited for the identification of the location of the ore zone than that of Cu. The results of the MMI method will be compared to the other partial extraction and total analyses

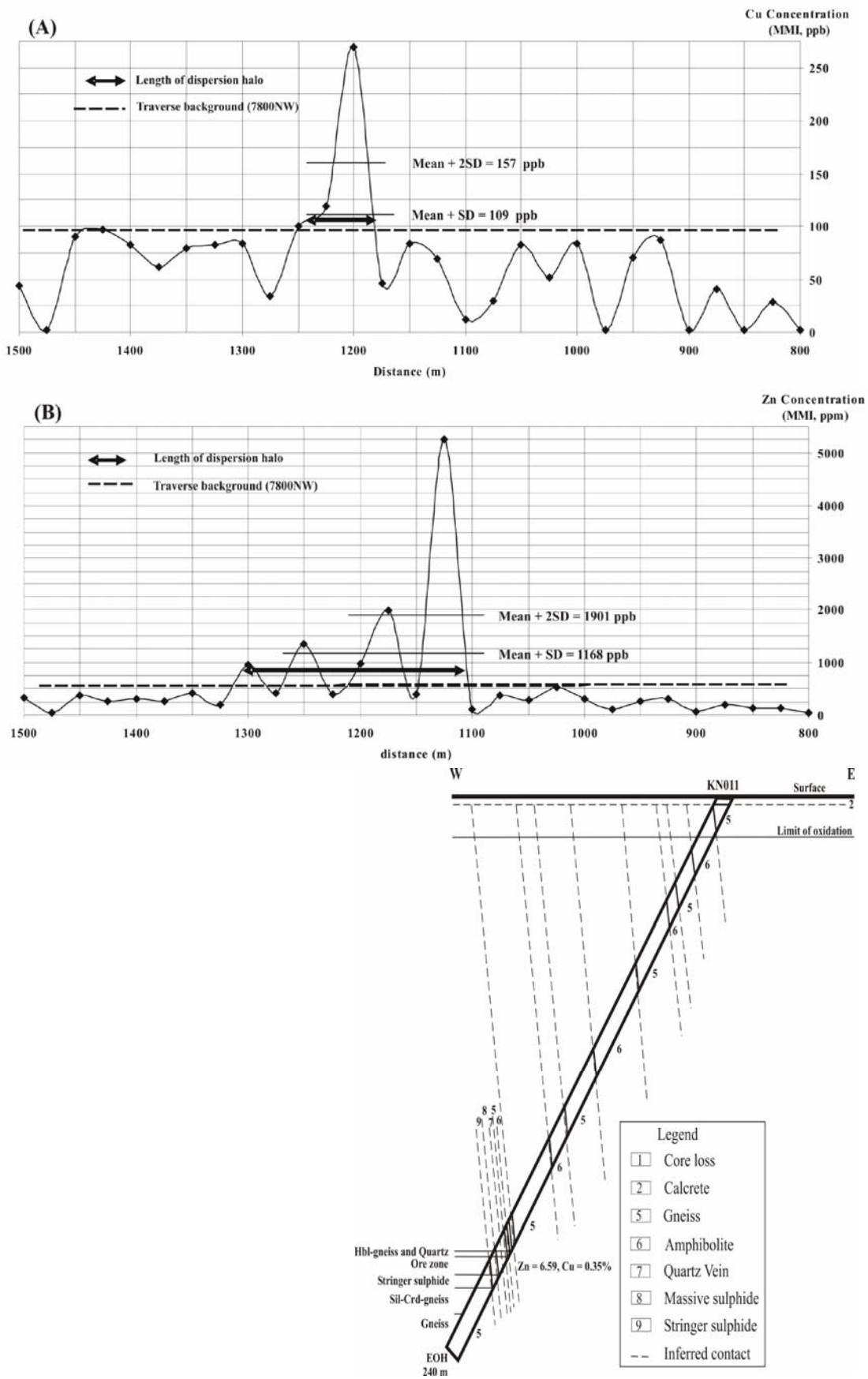

Figure 6.32: Variation of Cu (A) and Zn (B) in the regolith traverse 7800NW, MMI method (Sil: sillimanite; Crd: cordierite and Hbl: hornblende)

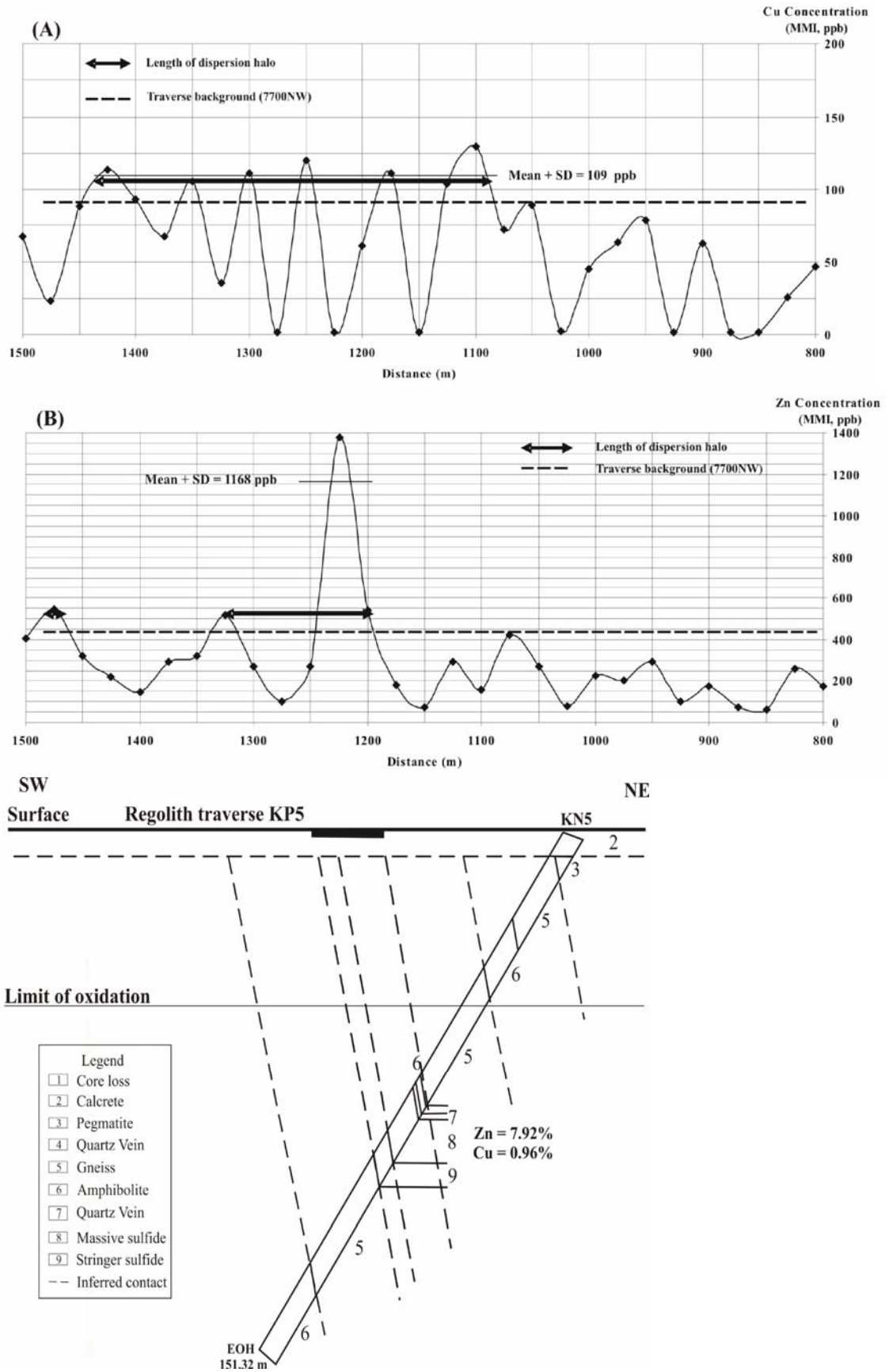

Figure 6.33: Variation of Cu (A) and Zn (B) in the regolith traverse 7700NW, MMI method.

techniques in the next section.

6.6.4. Comparison of NH_4EDTA, MMI and XRF methods

Different analytical methods such as total analysis by XRF and partial analyses using the MMI technique and NH_4EDTA extractions analyzed by ICP-MS were used in previous sections to identify anomalous sand samples located above buried sulphide mineralization. To compare the results, the peak to background ratio is calculated for comparison in Table 6.21, where the background value is estimated for the individual length of the traverse. The dispersion halo for Zn as determined from the MMI results shows a larger span, followed by ICP-MS and finally XRF. For the Cu halo, the NH_4EDTA method exhibits the largest span then XRF and then MMI. The largest span for Mn is shown by NH_4EDTA (ICP-MS) method followed by XRF. The XRF method shows the largest span for Pb and S in comparison to NH_4EDTA (ICP-MS).

In some cases the peak to background ratio is high (KP12, NH_4EDTA for Pb, etc), but the length of the dispersion halo is small. In reconnaissance exploration, the size of the dispersion haloes is more important than the peak to background ratio. Cu and Zn show the widest dispersion haloes when compared to those of other elements and oxides.

Table 6.21: Anomaly to background ratio of different analytical methods for Cu, Zn, Pb, Mn and S

Analytical Method	Regolith Traverse	Element (unit)	Background Value	Peak Value	P/B ratio[1]	Length of dispersion halo (m)
XRF	KP12	Cu (ppm)	25	33	1.32	50
		Zn (ppm)	104	138	1.33	110
		Pb (ppm)	17	22	1.29	110
		MnO (%)	0.1	0.12	1.20	75
		S (ppm)	22	205	9.32	110
	T2	Cu (ppm)	28	86	3.07	130
		Zn (ppm)	93	174	1.87	70
		Pb (ppm)	23	53	2.30	100
		MnO (%)	0.07	0.12	1.71	80
		S (ppm)	220	1900	8.64	80
NH_4EDTA (ICP-MS)	KP12	Cu (ppb)	3750	5500	1.47	70
		Zn (ppb)	5500	9552	1.74	70
		Pb (ppb)	8	120	15	25
		Mn (ppm)	109	191	1.75	110
		S (ppm)	20	182	9.10	25
	T2	Cu (ppb)	4500	34590	7.69	170
		Zn (ppb)	9600	33638	3.50	160
		Pb (ppb)	3400	7327	2.16	150
		Mn (ppm)	62	346	5.58	70
		S (ppm)	11	20	1.82	110
MMI	7700NW	Zn (ppb)	445	1380	3.10	125
	7800NW	Zn (ppb)	650	5265	8.10	200
		Cu (ppb)	90	270	3	50

Note: 1: peak to background ratio; Background = traverse background value

This study came to different conclusions regarding the size of the dispersion halo that can be detected at the two investigated deposits. At Kantienpan were the sand cover is

very shallow to absent, dispersion appears to be related to the secondary redistributions of gossaniferous clasts rather than dispersion of mobile metal ions on the surface of sand particles. The total analytical approach (XRF method) shows a wider dispersion halo than methods based on partial extraction. Whereas, at Areachap, where relatively thick sand (approximately one meter) covers the calcrete layer, partial extraction (based on a NH_4EDTA solution) results in a larger, recognizable, dispersion halo than that, that could be detected by total analysis (XRF).

6.7. Dispersion of the elements of interest in the calcrete environment

Vermaak (1984) studied the calcrete in the Areachap, Copperton, Jacomynspan and Hartebeestpan areas and the following conclusions were derived from his findings:

- Calcretes associated with the gossan above the ore zone display anomalous ore-related element concentrations (Cu, Zn and Pb).
- Dispersion of the ore-related elements is largely restricted to the calcrete directly overlying the ore zone.
- The concentration of the ore-related elements increase with depth above the ore zone.
- Calcrete with gossan inclusions, where the gossan was removed by hand picking, shows elevated concentrations of the ore-related elements.
- That the ore related elements are weakly dispersed in the calcite, but are concentrated in the other constituents of the calcrete as confirmed by comparing XRF analyses with the analyses of the HCl soluble component by atomic absorption.
- EDTA extractions does not effectively discriminate between samples with a high total Cu, Zn and Pb contents based on XRF analyses.

The current investigation intends to the further study of the calcretes by establishing the actual host of the elements of interest such as Cu, Zn, Pb and S in the calcrete environment. The question asked is if these elements are dispersed into the calcrete itself, or if they are confined to the distribution of gossan inclusions. Should the former be the case, calcrete may have to be sampled in future geochemical exploration programmes. On the other hand, the identification of gossan material may be regarded as an alternative to indication of the presence of concealed mineralization. In this regard it is important to

refer to the study of McQueen et al. (1999) where it was found that Au could be found in the low Mg-calcite of calcrete from southeastern Australia.

The calcrete of this area is mainly composed of a calcite (low Mg), and quartz as determined by XRD (Table 6.23). The calcite is expected to buffer surface water at relatively high pH conditions and therefore lower the solubility of base metals, limiting the mobility of these elements (Cu, Zn and Pb). In their experiment Mann et al. (1995) and Mann et al. (1997) have shown that varying quantities of calcium carbonate placed artificially as a single layer on top of sand does not prevent the solution from transmitting a base metal anomaly from the underlying material to the overlying sand. In the current study, this finding is tested under natural conditions where the anomaly related to the weathered massive sulphide deposit is separated from overlying eolian sand by a calcrete layer of substantial thickness.

The objective of sampling the calcrete is to investigate if these metals may remain sufficiently mobile in the groundwater of the secondary environment to be transported to surface under these high pH conditions. For this the variations in the concentration of the elements of interest in the calcrete layer are investigated with depth.

6.7.1. Kantienpan calcrete samples

To investigate the mobility of the elements of interest in the calcrete, it is important to discriminate between the base metals contained in gossan clasts in the calcrete and those dispersed in the calcrete itself. Two possible ways by which the calcrete and gossan fragments could be investigated separately were considered here, namely selective dissolution as done by Vermaak (1984) and physical separation using magnetic properties. Because of the potential contamination of the chemical solutions by these elements contained in materials displaying variable solubility under different physical condition that effect the solution, it was decided to investigate the dispersion of the ore related elements in the calcite part of the calcrete. It is unpractical to determine the concentrations of elements of which the abundances are in the parts per million range by microprobe analysis. It was therefore decided to analyze the calcrete by XRF after the physical separation of the calcite rich portion from the gossan rich material. For this purpose, the magnetic component of the calcrete sample was separated first by hand sorting and then by using a hand magnet followed by a Frantz

isodinamic magnetic separator (see Appendix D for detail). The results of the XRF analysis on the magnetic and non-magnetic parts of sample KP12/4 are given in Table D.19 (Appendix D). Assuming that most of the Ca and Mg present in the sample would be in a carbonate form and the Ca and Mg contents (normally expressed as oxides) were recalculated as carbonates.

Table 6.22: The comparison of major and trace elements of interest in visually cleaned, magnetic and non-magnetic parts of calcrete sample KP12/4, Kantienpan (A: ampere)

Major (%)	Visually clean	Non-magnetic part of sample			Magnetic part of sample				
		Completely clean		Clean[1]	Hand magnet	0.1A	0.3A	0.5-0.9A	1.1-1.7A
	KPR 12/4	Non-Mag1	Non-Mag2	Non-Mag3	Mag1	Mag2	Mag3	Mag4	Mag5
$CaCO_3$ *	70.25	71.09	75.00	71.36	75.75	71.29	72.80	72.73	72.46
SiO_2 *	18.43	16.84	13.84	15.56	12.67	12.71	12.42	13.79	14.69
TiO_2 *	0.22	0.09	0.1	0.15	0.21	0.51	1.1	0.98	0.53
Fe_2O_3 *	1.52	0.74	0.74	1	1.61	9.99	3.2	3.3	2.14
$MgCO_3$ *	5.35	5.04	4.90	5.26	5.09	5.64	5.14	5.62	5.83
Al_2O_3 *	2.54	1.99	1.91	2.05	1.91	1.92	1.94	2.35	2.66
Na_2O *	0.23	0.24	0.24	0.23	0.23	0.27	0.27	0.28	0.28
K_2O *	0.71	0.66	0.58	0.64	0.57	0.41	0.44	0.49	0.56
TOTAL	99.25	96.69	97.31	96.25	98.04	102.74	97.31	99.54	99.15
Trace elements (ppm)									
Cu	20	12	8	12	5	6	11	14	13
Pb	4	3	3	6	3	16	3	4	3
Zn	45	42	39	52	42	70	86	68	62
S *	513	578	363	1142	446	289	300	299	329
V	35	16	18	19	37	305	72	63	46

Note: KPR12/4 is the original sample, *: semi-quantitive analysis, 1: Cleaned by hand magnet

The fact that the recalculated total sum of major elements shown in Table 6.22 is much closer to the ideal 100% shows that this is a valid assumption. These samples contain 70.25 to 75.75% $CaCO_3$, 12.4 to 18.4% SiO_2, 0.74 to 10% Fe_2O_3, 5.04 to 5.83% $MgCO_3$ and 1.9 to 2.7% Al_2O_3 as based on semi-quantitative major element XRF powder analyses. In terms of trace elements, non-magnetic parts (sample Non-Mag1 and 3) have the highest concentration of S (Table 6.22). However, in some of the other samples higher S contents were observed in the magnetic fractions (KP12/2 and KP12/3, Table 6.24) and it must be concluded that the results on the S distribution remains inconclusive. The magnetic separate has higher Zn, Cu, Pb and V contents when compared to the original and non-magnetic samples (Table 6.22). Based on the results of this table, the Frantz isodinamic magnetic separator did not give a significant improvement on the purity of the calcite rich material separated visually. The sample cleaned with the Frantz separator (Non-Mag 1 and 2) does not result in a marked improvement when comparing its composition with the visually cleaned sample (KP12/4, after hand separation). It was decided to use only visually

cleaned calcrete material for further investigation, since these results would also be easy to reproduce and cost efficient during an exploration campaign.

To identify the mineralogy of the calcrete sample in the magnetic and non-magnetic parts, and to also identify the host mineral of the elements of interest, XRD analyses were done on both magnetic and non-magnetic parts of the separate and the results are listed in Appendix E. The different minerals present in the magnetic and non-magnetic parts of a calcrete sample KPR12/4 as determined by quantitative XRD are given in Table 6.23.

Table 6.23: The different minerals in the visually cleaned, magnetic and non-magnetic parts of a calcrete sample (KPR12/4, Kantienpan) as determined by quantitative XRD.

Sample	Cal	Q	Mc	Ab	Ms	Ilm	Hem	Mgt	Act	Reference
KPR12/4	77.09	13.10	2.84	4.20	2.78	-	-	-	-	Original Sample
Non-Mag 1	75.59	12.17	5.51	4.96	1.77	-	-	-	-	Reza2
Non-Mag 2	75.15	11.69	6.45	4.39	2.32	-	-	-	-	Reza12
Non-Mag 3	73.21	13.91	6.05	4.72	2.11	-	-	-	-	Reza1
Mag 1	77.24	10.36	5.61	4.89	1.55	-	-	0.35	-	Reza13
Mag 2	78.04	9.75	4.85	1.88	0.87	-	1.73	2.56	-	Reza3
Mag 3	77.92	9.24	3.93	5.05	2.09	0.9	-	-	0.44	Reza4
Mag 4	78.89	7.52	3.75	5.93	1.88	0.87	-	-	1.17	Reza5
Mag 5	75.65	8.70	5.78	6.46	2.89	0.23	0.29	-	-	Reza6

Cal: calcite, Q: quartz, Mc: microcline, Ab: albite, Ms: muscovite, Ilm: Ilmenite, Hem: hematite, Mgt: magnetite, and Act: Actinolite

The non-magnetic part of the sample contains calcite, quartz and alkali feldspars, whereas the magnetic part of sample comprises calcite and some quartz and alkali feldspars together with the hematite and magnetite minerals (Table 6.23). This is most probably due to the difficulty of liberating the different minerals in the calcrete material. Table 6.23 demonstrates that albite and microcline are concentrated in the non-magnetic fractions. Calcite is present in both the magnetic and non-magnetic fractions of the sample. Quartz, relative to calcite, is more abundant in the nonmagnetic fraction. Magnetite and hematite, presumably related to the gossan component of the sample, are extracted in the first and second magnetic separates. Ilmenite and actinolite are present in the higher current magnetic fractions of the calcrete sample in very low concentrations. Cu is associated with the iron oxides, but

seems to be dispersed in the rest of the sample as well. This conclusion is substantiated by the results of the other samples (Table 6.23), showing that Cu may be concentrated in the hematite/magnetite (iron rich) components of the samples. Distribution of Zn appears to be more strongly related to the distribution of magnetite, although some of the Zn may also be dispersed in the other iron-bearing fractions of the sample. Pb may be directly associated with the distribution of magnetite in Table 6.22. But the abundance of Pb is low in the other samples (Table 6.24) and no significant conclusion could be reached. Finally, the distribution of V appears to be strongly related to the distribution of magnetite (Tables 6.22 and 6.24).

The variation of major oxides and trace elements for the visually cleaned calcrete samples taken from the surface at Kantienpan are given in Table 6.24.

Table 6.24: The comparison of major oxides and trace elements of interest in visually cleaned parts of calcrete samples in the Kantienpan (A: ampere and *: semi-quantitative analyses)

Major elements(%)	Visually clean calcrete samples					
	Major oxides (%)					
	KPR12/1	KPR12/2	KPR12/3	KPR 12/4	KPR12/5	KPR12/6
$CaCO_3$ *	77.32	78.88	83.27	70.25	70.93	79.20
SiO_2 *	14	11.79	9.44	18.43	16.59	11.34
TiO_2 *	0.1	0.15	0.12	0.22	0.19	0.16
Fe_2O_3 *	0.79	1.48	1.54	1.52	2.31	3.05
$MgCO_3$ *	6.02	6.07	4.15	5.35	5.95	4.15
Al_2O_3 *	1.22	1.68	1.23	2.54	2.42	2.01
Na_2O *	0.18	0.19	0.19	0.23	0.24	0.2
K_2O *	0.33	0.51	0.29	0.71	0.72	0.45
TOTAL	99.96	100.75	100.23	99.25	99.35	100.56
Trace elements (ppm)						
Cu	9	19	32	20	17	49
Pb	3	5	9	4	7	4
Zn	40	95	117	45	62	210
S*	532	488	601	513	469	495
V	26	28	28	35	37	60

These samples contain 70.25 to 83.27 % of $CaCO_3$, 9.4 to 18.43 % SiO_2, 1.22 to 2.54 % Al_2O_3, 4.15 to 6.07 % $MgCO_3$ and 0.79 to 2.31 % Fe_2O_3 contents based on semi-quantitative XRF powder analyses. Samples KP12/3 and KP12/6 are from the gossan-bearing zone, and shown the highest Cu, Zn, S and V contents as determined by quantitative (Cu, Zn and V) and semi-quantitative (S) XRF analyses.

6.7.2. Areachap calcrete samples

To investigate the variation of selected trace elements in the calcrete layer, two profiles were sampled (grab samples) in the calcrete layer as exposed in an old

excavation at the Areachap deposit (Fig. 6.34 A and B). A gossan zone with malachite-filled veinlets occurs at the bottom of this layer (Fig 6.34 C). The gossan zone at Areachap display fractures filled with what appears to be Dwyka tillite. If this is the case it would imply that the gossan formed before the denudation as result of the glaciation at the onset of the Karoo sedimentation. Following the erosion of the Karoo sediments the entire area was covered with a thick layer (three to six meters) of calcrete, which in turn is overlain by wind blown Kalahari sand deposits. Within the calcrete layer, there are blocks and fragments of the silicified gossan material, distributed from the bottom of the layer to surface. The sampling profiles were positioned so as to avoid the larger gossan fragments.

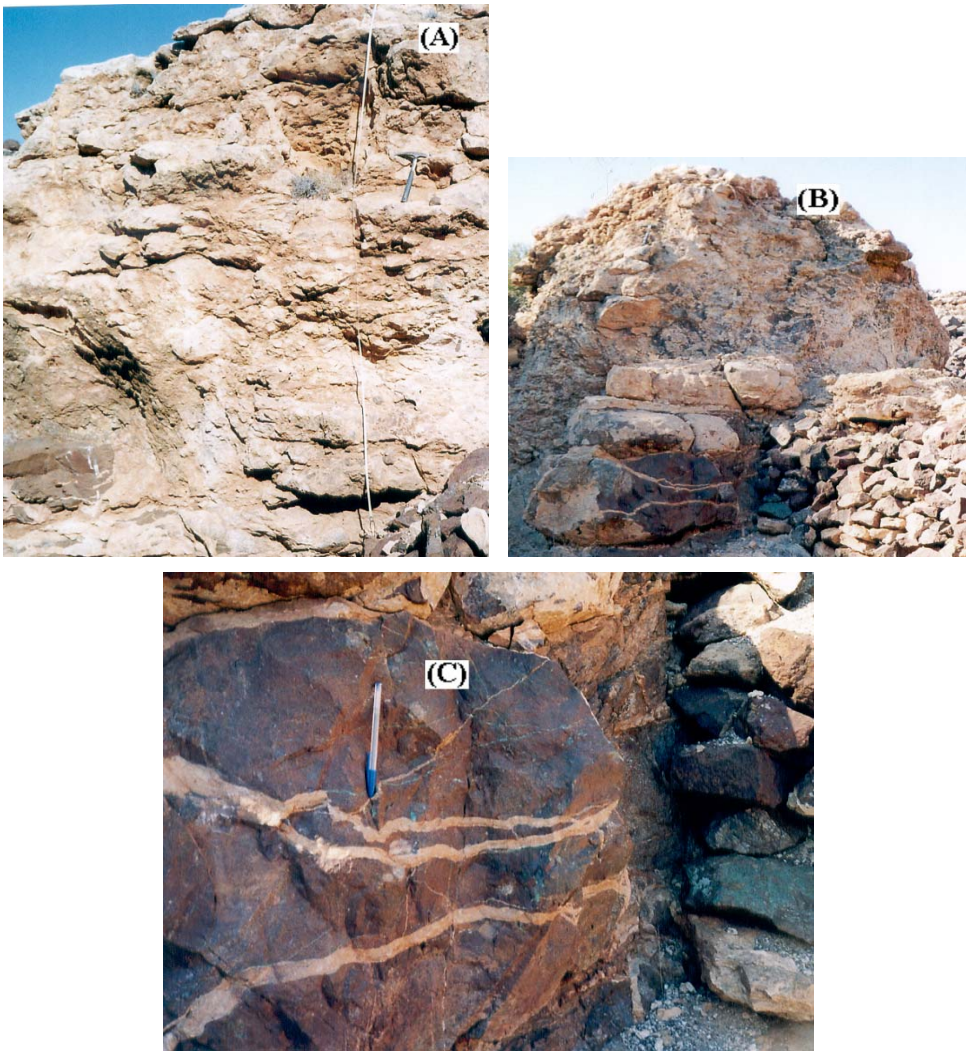

Figure 6.34: The calcrete layer in an old excavation at Areachap. Calcrete profile Calc1 (A), Calc2 (B) and a gossan rock with malachite and calcrete-filled veinlets at the bottom of calcrete layer (C).

XRF results of the original and magnetic separates of one of these profiles (Calc1) are given in Table D.22 (Appendix D). In Figure 6.35, the variation of major oxides versus depth is shown for the non-magnetic parts of the original samples (visually clean calcrete). They are composed of 54.98 to 83.34 % $CaCO_3$, 10 to 26.52 % SiO_2, 1.43 to 6.24 % Al_2O_3, 3.36 to 5.69 % $MgCO_3$ and 0.91 to 4.77 % Fe_2O_3 based on semi-quantitative XRF powder analyses.

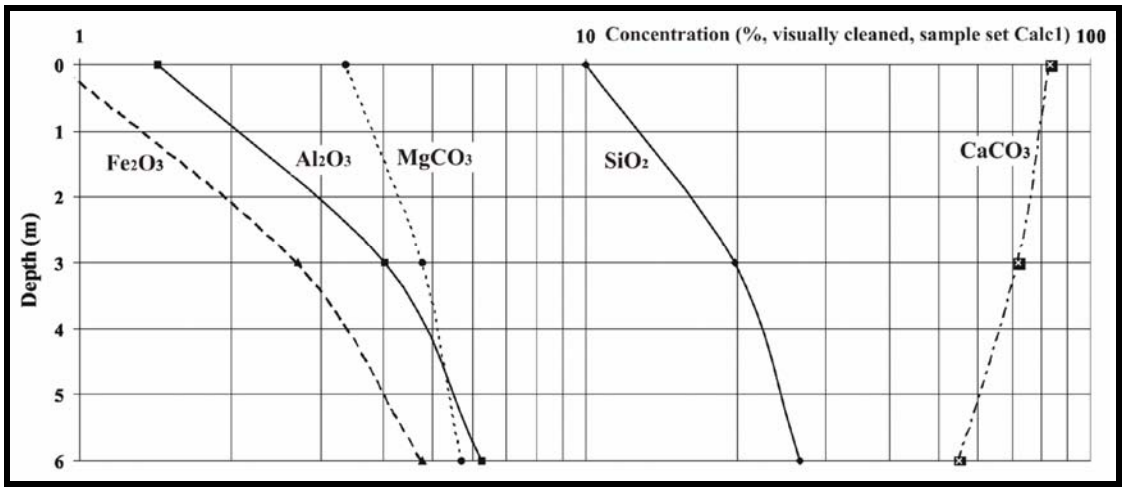

Figure 6.35: Major oxides variation versus depth in the Areachap calcrete layer (visually cleaned samples referred to as Calc1).

The variations of Cu, Zn, Pb and S as determined by quantitative (Cu, Zn and Pb) and semi-quantitative (S) XRF analyses versus depth in original calcrete samples (visually clean calcrete) for the same sample profile (Calc1) are shown in Figure 6.36. Based on this figure, Cu, Zn and Pb contents increase with depth. The concentrations of these elements are therefore much lower at surface than deeper down the calcrete profile. It may be concluded that the peak to background ratio of anomalies in surface samples would depend on the thickness of the underlying calcrete layer. S does not show the same trend as Cu, Zn and Pb. This may be explained by the presence of different types of sulphur phases in the sample, i.e., sulphates as a result of ground water compositions and the evaporation processes and sulphates as remnants of the oxidized primary sulphide minerals. It should also be considered that sulphates may accumulate in the surface environment due to the interaction of rain water, groundwater and evaporation processes such as seen in pan formation. This may result in false S anomalies not related to underlying sulphide mineralization.

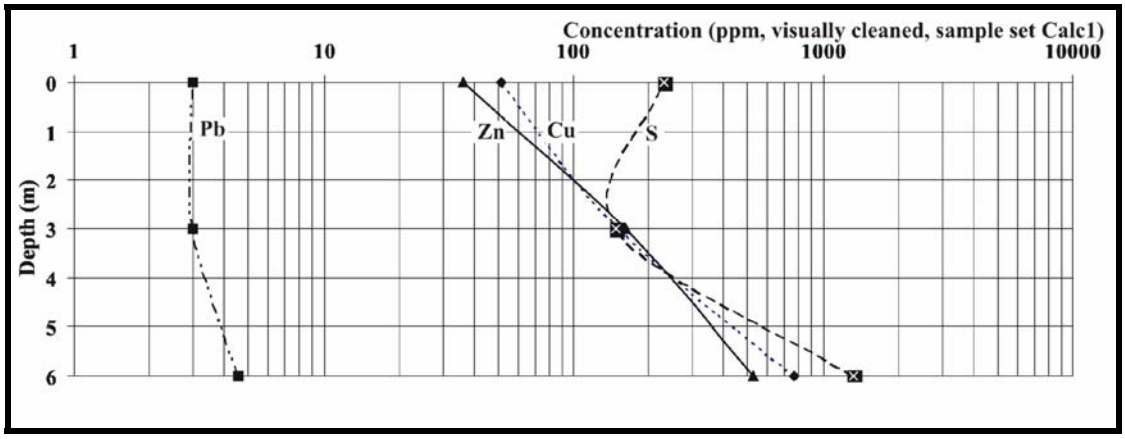

Figure 6.36: Variation of Cu, Zn, Pb and S versus depth in the Areachap calcrete layer, (visually cleaned samples referred to as Calc1).

Figure 6.35 and 6.36 display an increasing trend of trace elements (Cu, Zn and Pb) and major oxides such as Al_2O_3, $MgCO_3$, SiO_2 and Fe_2O_3 with depth. This may be seen as evidence that the calcrete formation was superimposed on a weathered soil profile and that the calcrete does not merely represent calcretized Kalahari sand. This interpretation is also supported by the observation that gossan clasts are enclosed directly above the ore zone in the calcrete over the entire thickness of the calcrete layer. It is expected that the primary mineral phases present would be the same as determined for Kantienpan namely calcite, quartz, albite and microcline.

The chemical composition of calcrete in sample set Calc2 in the Areachap area are given in Table D.23 (Appendix D). In Figure 6.37, the variation of major oxides versus depth in this area is shown (original samples). They contain 48.89 to 63.89 % $CaCO_3$, 8.12 to 25.8 % SiO_2, 1.41 to 11.36 % Fe_2O_3, 1.68 to 7.3 % Al_2O_3 and 3.22 to 6.55 % $MgCO_3$ contents based on semi-quantitative XRF powder analyses.

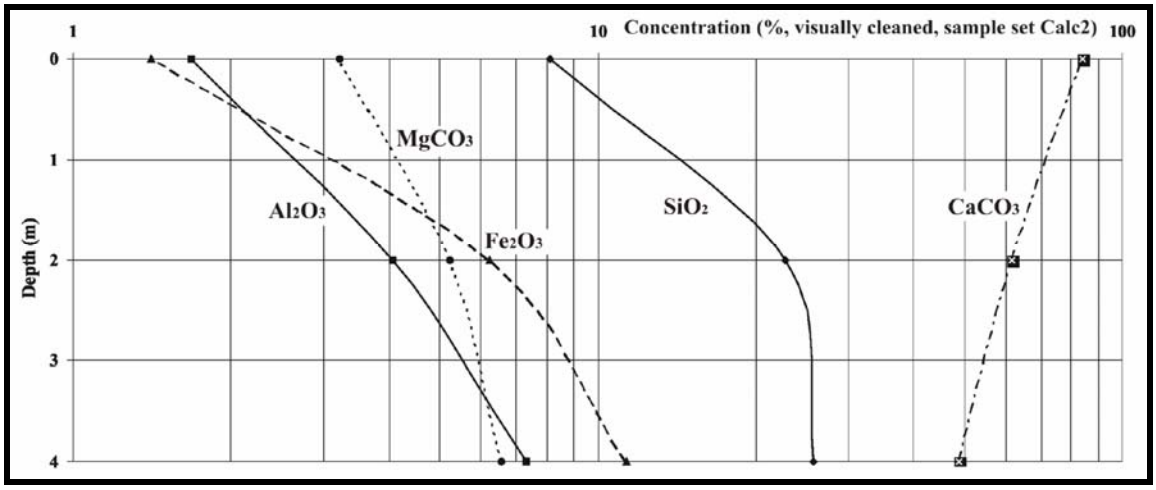

Figure 6.37: Major oxides variation versus depth (visually cleaned samples referred to as Calc2) in the Areachap.

The variations of trace elements in the original samples are demonstrated in Figure 6.38 (for sample set Calc2) as determined by quantitative (Cu, Zn and Pb) and semi-quantitative (S) XRF analyses. Based on this figure, Zn and Pb contents increase with depth, but Cu and S contents decrease. The highest content of S occurs at the surface and the lowest content at a depth of 4 m. Trace elements, such as Pb and Zn, and major oxides, i.e. Al_2O_3, $MgCO_3$, SiO_2 and Fe_2O_3 show the same trend.

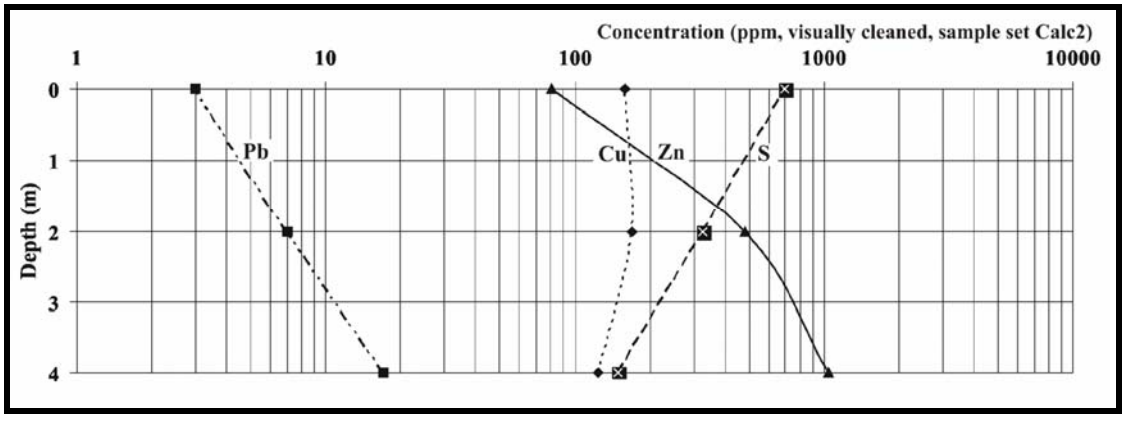

Figure 6.38: Variation of Cu, Zn, Pb and S versus depth in the calcrete layer, Areachap (visually cleaned samples referred to as Calc2).

The concentration of trace elements in calcrete samples at the surface therefore depends on the thickness of the calcrete layer in the area.

6.7.3. Comparison of calcretes close to the ore zone and further away

In this section the composition of calcrete samples collected from above the ore zone (anomalous samples, Calc1-3 and Calc2-3) are compared to samples (Vcal2 and Vcal3) that were collected away from any known mineralization (background samples). XRF results of these samples are given in Tables D.24 and D.25 (Appendix D). Some of the calcrete samples (Table D.26) provided by Vermaak (1984) from Areachap and Copperton Cu-Zn Mine and further away from the known mineralization are also used here. These samples include of the calcrete and complex calcrete, which are calcrete samples that contain gossan particles. The average values of the elements and oxides for these samples are used for plotting in the three angular diagrams.

In Table 6.25 the chemical composition of the original calcrete samples near the ore zone in the study area is compared to calcrete samples further away from the ore zone. In Figure 6.39, the chemical composition of original calcretes above the ore zone and data set of Vermaak (1984) is compared to that of those samples collected further away from the known mineralization. Based on this figure, the calcrete samples near the ore zone are enriched in $CaCO_3$, Cu and Zn and samples collected further away from the known mineralization are enriched in V and Sr. The latter samples have higher Na_2O and K_2O contents when compared to the calcrete samples close to the ore zone. Calcretes directly related to massive sulphide mineralization may be discriminated from those developed in areas away from the mineralization by plotting the V-Cu-Zn and Sr-Cu-Zn contents in triangular diagrams as presented in Figure 6.39, A and B.

Table 6.25: Chemical composition of visually cleaned calcretes near the ore zone (Calc1-3 and Calc2-3 at Areachap) and further away from the mineralized zone (Vcal2 and Vcal3)

Major oxides (%)	Original calc1-3	Original Calc2-3	Original Vcal2	Original Vcal3
SiO_2 *	10.01	8.12	18.2	12.9
$MgCO_3$ *	3.36	3.22	7.44	7.44
$CaCO_3$ *	83.34	83.89	69.64	76.25
Na_2O *	0.14	0.19	0.3	0.2
K_2O *	0.25	0.33	0.5	0.4
Trace elements (ppm)				
Cu	52	159	2	2
Pb	3	3	3	3
Sr	114	158	149	236
Zn	36	81	29	30
S *	229	699	294	231
Sc	1	1	<1	<1
V	19	28	24	41
Depth	Surface	Surface	Surface	Surface

*: Semi-quantitative analysis

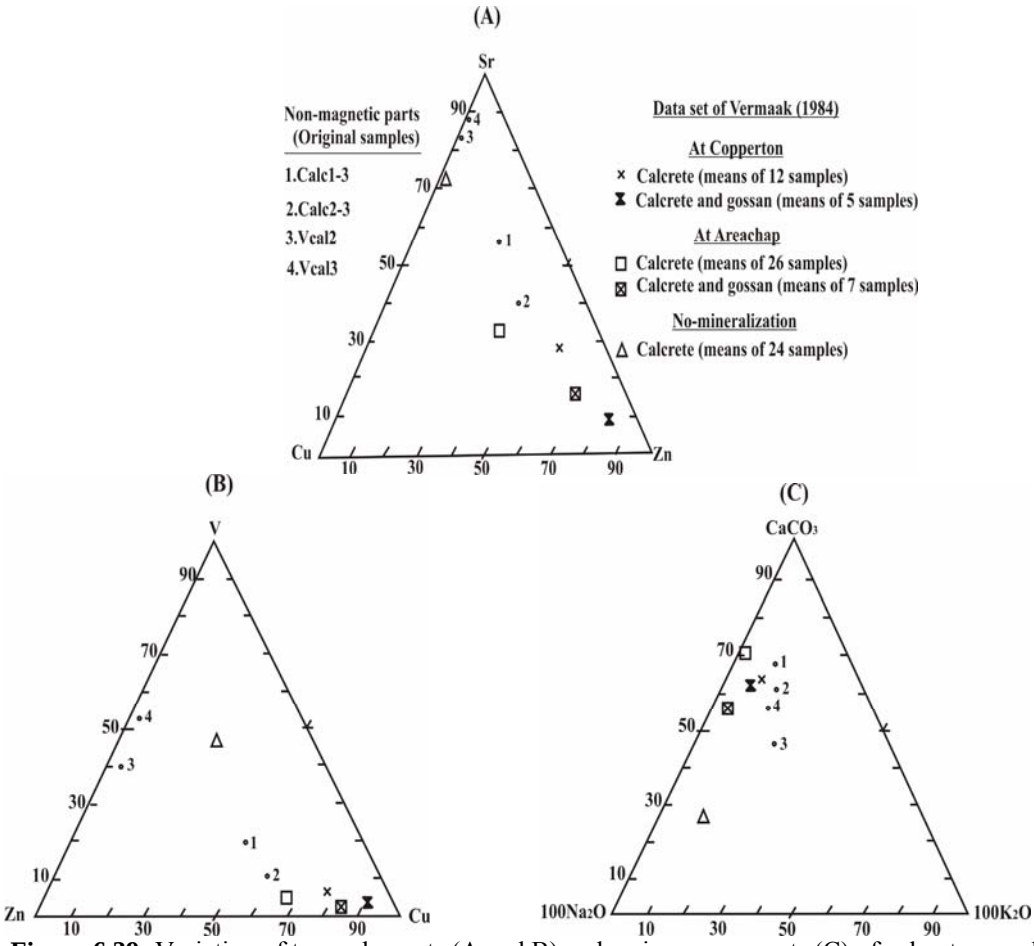

Figure 6.39: Variation of trace elements (A and B) and major components (C) of calcrete samples close to ore deposit and further away from the mineralized zone.

It is concluded that the trace elements contents in soil or sand samples directly overlying the calcrete would depend to the thickness of the calcrete layer above the ore deposit. A very thick layer of calcrete may not allow for much dispersion of the elements of interest in trace elements in the surface sands. These elements may be concentrated in non-magnetic and magnetic part of calcrete. Based on this research, mineralogical composition of the non-magnetic part of the calcrete contains of calcite, quartz and microcline and the magnetic part comprises of magnetite, hematite, calcite and albite (at Kantienpan).

It could therefore be demonstrated that calcrete samples close to the ore zone have higher contents of Cu, Zn and $CaCO_3$ when compared to the calcrete samples further away from the ore zone and lithogeochemical exploration programme based on the visually cleaned calcrete samples may therefore lead to the successful identification of underlying mineralization, but the dispersion of the elements of interest may be severely restricted.

It is however evident that these elements are available at the calcrete-sand interface and that these elements of interest could then be dispersed in the sand by ground and rain water as in the case of mobile metal ions.